

2017

In vivo inhibition of tryptophan catabolism reorganizes the tuberculoma and augments immune-mediated control of *Mycobacterium tuberculosis*

Shabaana A. Khader

Washington University School of Medicine in St. Louis

Follow this and additional works at: https://digitalcommons.wustl.edu/open_access_pubs

Recommended Citation

Khader, Shabaana A., "In vivo inhibition of tryptophan catabolism reorganizes the tuberculoma and augments immune-mediated control of *Mycobacterium tuberculosis*." *Proceedings of the National Academy of Sciences of the United States of America*. 115, 1. E62-E71. (2017).

https://digitalcommons.wustl.edu/open_access_pubs/6482

This Open Access Publication is brought to you for free and open access by Digital Commons@Becker. It has been accepted for inclusion in Open Access Publications by an authorized administrator of Digital Commons@Becker. For more information, please contact engeszer@wustl.edu.



In vivo inhibition of tryptophan catabolism reorganizes the tuberculoma and augments immune-mediated control of *Mycobacterium tuberculosis*

Uma S. Gautam^a, Taylor W. Foreman^{a,b,1}, Allison N. Bucsan^{a,b}, Ashley V. Veatch^a, Xavier Alvarez^a, Toidi Adekambi^c, Nadia A. Golden^a, Kaylee M. Gentry^a, Lara A. Doyle-Meyers^a, Kasi E. Russell-Lodrigue^a, Peter J. Didier^a, James L. Blanchard^a, K. Gus Kousoulas^{d,e}, Andrew A. Lackner^{a,b,2}, Daniel Kalman^{d,e}, Jyothi Rengarajan^c, Shabaana A. Khader^f, Deepak Kaushal^{a,b,3}, and Smriti Mehra^{a,d,e,3}

^aTulane National Primate Research Center, Tulane University School of Medicine, Covington, LA 70433; ^bDepartment of Microbiology & Immunology, Tulane University School of Medicine, New Orleans, LA 70112; ^cEmory Vaccine Center, Emory University, Atlanta, GA 30322; ^dDepartment of Pathobiological Sciences, Louisiana State University School of Veterinary Medicine, Baton Rouge, LA 70803; ^eCenter for Experimental Infectious Disease Research, Louisiana State University School of Veterinary Medicine, Baton Rouge, LA 70803; and ^fDepartment of Molecular Microbiology, Washington University in St. Louis, St. Louis, MO 63130

Edited by Barry R. Bloom, Harvard T. H. Chan School of Public Health, Boston, MA, and approved November 6, 2017 (received for review June 28, 2017)

***Mycobacterium tuberculosis* continues to cause devastating levels of mortality due to tuberculosis (TB). The failure to control TB stems from an incomplete understanding of the highly specialized strategies that *M. tuberculosis* utilizes to modulate host immunity and thereby persist in host lungs. Here, we show that *M. tuberculosis* induced the expression of indoleamine 2,3-dioxygenase (IDO), an enzyme involved in tryptophan catabolism, in macrophages and in the lungs of animals (mice and macaque) with active disease. In a macaque model of inhalation TB, suppression of IDO activity reduced bacterial burden, pathology, and clinical signs of TB disease, leading to increased host survival. This increased protection was accompanied by increased lung T cell proliferation, induction of inducible bronchus-associated lymphoid tissue and correlates of bacterial killing, reduced checkpoint signaling, and the relocation of effector T cells to the center of the granulomata. The enhanced killing of *M. tuberculosis* in macrophages in vivo by CD4⁺ T cells was also replicated in vitro, in cocultures of macaque macrophages and CD4⁺ T cells. Collectively, these results suggest that there exists a potential for using IDO inhibition as an effective and clinically relevant host-directed therapy for TB.**

macaque | tuberculosis | granuloma | IDO | T cell

There is an urgent need to improve antitubercular treatment strategies. Tuberculosis (TB) continues to result in close to two million deaths worldwide on an annual basis, and is the single biggest killer of AIDS patients (1). Additionally, ~10% of newly diagnosed patients exhibited disease with some resistance to anti-TB drugs, ranging from multidrug-resistant to extensively drug-resistant TB (2). The failure to control TB stems from the lack of relatively poor understanding of both pathogenesis and the host factors that contribute to the susceptibility of TB disease. However, nonhuman primates (NHPs) recapitulate the complete breadth of the lung pathology and granulomatous responses that are emblematic of human disease (3). The granuloma is the site of host–*Mycobacterium tuberculosis* interactions, which either result in acute infection or the control of infection in a latent state (4). *M. tuberculosis* modulates these immune interactions to inhibit mycobacterial killing and therefore promote long-term survival of the bacilli.

The expression of indoleamine 2,3-dioxygenase (IDO) is dramatically enhanced in macaque granulomata (5). IDO catabolizes Tryptophan (Trp) to kynurenine (Kyn) and other metabolites, and acts to suppress the immune response, particularly the CD4⁺ T cell production of IFN- γ (6). Induction of host IDO is a nascent strategy to starve pathogens of Trp, an essential amino acid (7). However, *M. tuberculosis* can synthesize its own Trp de novo (8), potentially an adaption for its survival during Trp catabolism by

IDO in host phagocytes. Therefore, IDO production has little effect on mycobacterial metabolism and yet impacts protective host immune responses.

Here we demonstrate that increased IDO1 expression correlates with higher bacterial burden. Furthermore, IDO is particularly enriched in the macrophage-rich inner layer of the granuloma (5). This spatial expression may prevent lymphocytes, which are predominant in the external layers of the granuloma, from reaching the infected phagocytes, and this inhibition may further promote bacterial survival. We therefore hypothesize that the highly organized granulomas seen in NHPs and humans may be advantageous to *M. tuberculosis* due to this spatial exclusion

Significance

***Mycobacterium tuberculosis* induces the expression of the indoleamine 2,3-dioxygenase (IDO) enzyme, which catabolizes tryptophan. Tryptophan metabolites potentially suppress host immunity. The present study demonstrates that blockade of IDO activity reduces both clinical manifestations of tuberculosis (TB) as well as microbial and pathological correlates of the human TB syndrome in macaques. In granulomas, T cells localize in the periphery, and are unable to access the core, where bacilli persist. Inhibiting IDO activity altered granuloma organization such that more T cells translocated to the lesion core and exhibited highly proliferative signatures. Our results identify a highly efficient immunosuppressive mechanism at play in the granuloma environment that aids in *M. tuberculosis* persistence. The ability to modulate this pathway with safe and approved compounds could, however, facilitate chemotherapy-adjunctive host-directed therapy approaches for the control of TB.**

Author contributions: D. Kaushal and S.M. designed research; U.S.G., T.W.F., A.N.B., A.V.V., X.A., T.A., N.A.G., K.M.G., L.A.D.-M., K.E.R.-L., P.J.D., and J.L.B. performed research; U.S.G., T.W.F., A.N.B., D. Kalman, J.R., S.A.K., D. Kaushal, and S.M. analyzed data; and U.S.G., K.G.K., A.A.L., D. Kaushal, and S.M. wrote the paper.

The authors declare no conflict of interest.

This article is a PNAS Direct Submission.

This open access article is distributed under [Creative Commons Attribution-NonCommercial-NoDerivatives License 4.0 \(CC BY-NC-ND\)](https://creativecommons.org/licenses/by-nc-nd/4.0/).

Data deposition: The data reported in this paper have been deposited in the Gene Expression Omnibus (GEO) database, <https://www.ncbi.nlm.nih.gov/geo> [accession nos. [GPL10183](https://www.ncbi.nlm.nih.gov/geo/acc/show?acc=GPL10183) (macaque) and [GPL7202](https://www.ncbi.nlm.nih.gov/geo/acc/show?acc=GPL7202) (murine)].

¹Present address: Cellular Immunology Section, Vaccine Research Center, National Institute of Allergy and Infectious Diseases, NIH, Bethesda, MD 20892.

²Deceased April 2, 2017.

³To whom correspondence should be addressed. Email: dkaushal@tulane.edu or smehra@lsu.edu.

This article contains supporting information online at www.pnas.org/lookup/suppl/doi:10.1073/pnas.1711373114/-DCSupplemental.

of immune-protective lymphocytes. As such, the IDO pathway represents a potential target for host-directed therapy (HDT) to augment the control of TB.

Inhibitors of IDO activity [e.g., 1-methyl-tryptophan (1-MT, D-1MT)] are being evaluated as anticancer drugs. In this study, we demonstrated that D-1MT-mediated IDO inhibition resulted in somewhat increased *M. tuberculosis* killing, improved clinical signs of disease, increased lymphoid follicles and proliferation of pulmonary lymphocytes, and was associated with a drastic reorganization of the granuloma that allowed lymphocyte trafficking into the macrophage-tropic internal layers. These results lend significant credence to the utilization of IDO inhibitors as an HDT strategy adjunctive to anti-*M. tuberculosis* chemotherapy (9).

Results

IDO1 Is Expressed in a *M. tuberculosis* Burden-Dependent Manner in Infected Phagocytes and Experimental Hosts. We first studied whether IDO levels are induced in a *M. tuberculosis* burden-dependent manner. We found that IDO expression is induced in *M. tuberculosis*-infected murine (C3HeB/FeJ) bone marrow-derived macrophages (BMDMs) (Fig. 1A) and rhesus macaque BMDMs (Fig. 1B and Fig. S1) in vitro and in lungs of *M. tuberculosis*-infected C3HeB/FeJ mice (Fig. 1C and D). Furthermore, IDO expression levels were highly correlated with lung CFUs ($P = 0.02$, $r^2 = 0.68$) (Fig. 1E). We have recently shown that most animals with latent TB infection (LTBI) that were subsequently coinfecting with simian immunodeficiency virus (SIV), reactivated (10). In coinfecting animals, IDO levels largely

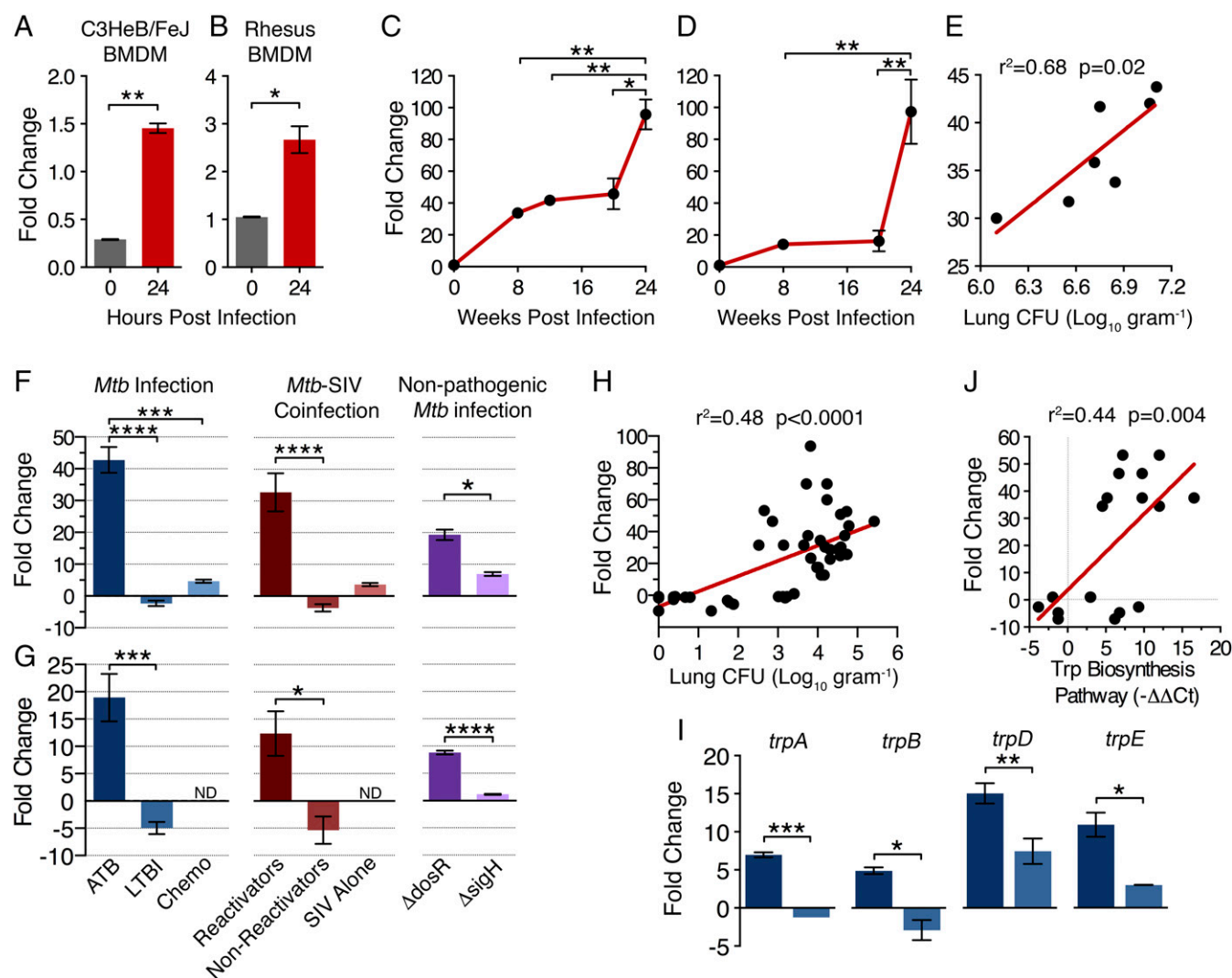


Fig. 1. Expression of IDO1 in vitro as well as in vivo experimental models of *M. tuberculosis* infection. IDO levels detected by qRT-PCR at 0 (gray) and 24 h (red) after *M. tuberculosis* infection relative to uninfected BMDMs from three biological replicates (A) C3HeB/FeJ mice (70) and (B) rhesus macaques (71). The average relative expression ($2^{-\Delta\Delta Ct}$) of IDO in C3HeB/FeJ mice lungs at weeks 8, 12–20, and 24 in respect to postday 1 (base line) *M. tuberculosis*-infected lungs by qRT PCR (C) and microarray (D) (70). Linear regression ($r^2 = 0.68$, $P < 0.05$) plot of IDO1 expression correlates to bacillary load in C3HeB/FeJ mice lungs at weeks 8 and 12 obtained is from C (E). IDO expression in the lung of rhesus macaques with ATB (dark blue bars), LTBI (intermediate blue bars), chemotherapeutic treatment of ATB (light blue bars), or nonpathogenic *M. tuberculosis* infection (dark and light purple bars) by qRT-PCR (F) and microarray (G). IDO expression in *M. tuberculosis*-infected (dark blue bars), LTBI-coinfecting SIV lungs either exhibited a reactivation (dark brown bars) or nonreactivation phenotype (light brown bars) (10). IDO expression in lungs of rhesus macaques infected with nonpathogenic *Mtb* Δ *dosR* (dark purple bars) or *Mtb* Δ *sigH* (light purple bars) (11, 13). Linear regression ($r^2 = 0.48$, $P < 0.0001$) plot of IDO expression correlates to bacterial burdens in the lungs of rhesus macaques with ATB (24–37 d postinfection) and LTBI (166–180 d postinfection) (H). Expression of Trp biosynthetic pathway genes in ATB (dark blue) and LTBI (light blue) animals (I) and their linear regression with IDO expression levels in ATB and LTBI animals ($r^2 = 0.41$, $P < 0.005$) (J). Data are means \pm SEM, * $P < 0.05$, ** $P < 0.01$, *** $P < 0.001$, **** $P < 0.001$ using (A, B, and I) Student's *t* test, (E, H, and J) linear regression analysis, or (C, D, F, and G) one-way ANOVA.

correlated with *M. tuberculosis* burdens (Fig. 1 *F* and *G*). Animals with TB exhibited an ~20- to 40-fold IDO induction relative to baseline, whereas the expression was unperturbed in animals that did not reactivate (Fig. 1 *F* and *G*) with high degree of concordance ($P < 0.0001$, $r^2 = 0.48$) (Fig. 1*H*). To effectively demonstrate IDO induction as a correlate of *M. tuberculosis* burden, we measured its expression in macaques receiving chemotherapy. Daily oral administration of moxifloxacin, ethambutol, and pyrazinamide, a multidrug-resistant regimen in humans, reduced IDO1 expression relative to untreated controls (Fig. 1 *F* and *G*). Consistent with the above findings, low IDO expression was observed in animals infected with nonpathogenic *M. tuberculosis* (*Mtb*) strains *Mtb* Δ *sigH* and *Mtb* Δ *dosR* (11–13) (Fig. 1 *F* and *G*). Lungs of animals infected with a high dose of *Mtb* Δ *sigH* mutant had reduced IDO levels (Fig. 1 *F* and *G*), which again demonstrates that IDO levels were driven by uncontrolled *M. tuberculosis* replication. Unlike *Mtb* Δ *sigH*, *Mtb* Δ *dosR* exhibits only partial attenuation, and adaptive immune responses are required for its control (13), likely explaining the intermediate expression of IDO in animals infected with *Mtb* Δ *dosR* (Fig. 1*G*). Hence, IDO is expressed in an *M. tuberculosis* burden-dependent manner. Concomitantly, the expression of the *M. tuberculosis* *tpA*, *tpB*, *tpD*, and *tpY* genes was induced in macaques with active TB (ATB) relative to LTBI (Fig. 1*I*). Thus, Trp biosynthesis is switched on in *M. tuberculosis* in vivo and correlates with host expression of IDO (Fig. 1*J*).

D-1MT Treatment Improves the Clinical Outcomes and Reduces Lung Tissue Pathology. Macaques recapitulate several aspects of human TB including ATB and LTBI (5, 11–26), HIV coinfection-mediated reactivation TB (10, 15), as well as immune protection (5, 21). We tested the importance of IDO signaling in vivo in acutely infected macaques by treating the animals with D-1MT, a specific inhibitor of IDO activity. Treatment was initiated 1 wk after *M. tuberculosis* infection (Fig. S2). The progression of TB was significantly altered in treated macaques, as reflected by clinical outcomes (Fig. 2). Whereas all of the control animals had to be killed within 5 wk of *M. tuberculosis* infection, D-1MT-treated animals survived until 8 wk, exhibited significantly delayed kinetics, and lower levels of serum C reactive protein (CRP) compared with controls (Fig. 2*A*). Similarly, treated animals exhibited limited weight loss over time compared with control animals (Fig. 2*B*). This finding was consistent with the low bacterial burdens detected in treated animals (Fig. 2 *C–E*). CFUs were determined from bronchoalveolar lavage (BAL) in two groups each at week 1 (the time when treatment was initiated), week 3 (i.e., 2 wk after treatment), and at the end point, at which time *M. tuberculosis* CFUs were also assessed in the lung tissues. The control animals exhibited significantly higher *M. tuberculosis* burdens ($P < 0.05$) in BAL at week 3 and in the terminal lung samples compared with the D-1MT-treated animals. BAL data are shown for at least three animals (Fig. 2*C*). However, the CFU levels in the BAL did not differ between the two groups at

week 1, before initiating treatment, indicating that the initial infections were similar (Fig. 2*C*). The total bacterial burdens in terminal lungs (Fig. 2*D*) and bronchial lymph node (BLN) (Fig. 2*E*) were significantly lower in D-1MT-treated animals than in the control animals (>1 log, $P < 0.05$). The bacterial burdens were also lower in liver, kidney, spleen in D-1MT-treated animals than controls (Fig. 2*E*). D-1MT-treated animals presented with fewer granulomas (Fig. 2*F*) relative to control animals (Fig. 2*G*) and exhibited significantly lower ($P < 0.005$) lung pathology (Fig. 2*H*). Hence, animals treated with D-1MT not only had better clinical outcomes (Fig. 2 *A* and *B*) and reduced pathology (Fig. 2 *F* and *H*), but also exhibited reduced bacterial burdens (Fig. 2 *C–E*). Together, these results underscore our contention that, although active TB developed in all animals, the disease in D-1MT-treated animals progressed more slowly and to a lesser extent.

D-1MT Treatment Reduces the IDO Enzymatic Activity. The central area of the BAL cytospin that contained regular, monolayer-distributed cells, as confirmed by H&E staining (Fig. S2), was used for Kyn staining on samples obtained from D-1MT-treated and control animals at week 3. Kyn is one of the end products of IDO enzymatic activity. Numerous studies have implicated it in the immunosuppressive function of this signaling pathway (27). It is also known to be a ligand for the aryl hydrocarbon receptor signaling pathway (28). Confocal microscopy revealed greater levels of Kyn accumulation in controls, relative to D-1MT-treated animals (Fig. 3*A*). Furthermore, quantification revealed a highly significant ($P = 0.0001$) fourfold reduction in the average number of Kyn⁺ cells in D-1MT-treated animals (Fig. 3*B*). We also quantified absolute levels of Kyn and Trp in the plasma, a second measure of IDO activity by ELISA using pure standards, and calculated the Kyn/Trp ratio as an indirect measure of IDO activity (Fig. 3*C*). The two groups had virtually indistinguishable Kyn/Trp ratios at week 1 (i.e., before the initiation of treatment). In week 3 plasma samples, however, a significantly different ($P < 0.001$) Kyn/Trp ratio was observed between two groups. Both results suggest that D-1MT treatment inhibits IDO enzyme activity ($> 95\%$ reduction) (Fig. 3*C*). The effect of D-1MT on IDO enzymatic activity could also be observed in the treated group of animals at later stages (up to week 8) during the infection (Fig. S2*B*). These results establish that the changes in disease progression in D-1MT-treated animals were correlated with inhibition of IDO.

Effect of the in Vivo Modulation of IDO Signaling on T Cell Phenotype. We phenotyped mononuclear cells isolated from dematrixed lung and BAL from the end point. Using these samples, we assessed temporal changes in both T cell numbers and T cell phenotypes in the lungs. BAL data at the end point was compared between two groups (Fig. 3 *D–H*), as previously described (10–13, 16, 20–23). The quantification of memory subsets was established for T cell populations based on CD28 and CD95 coexpression for which a representative flow cytometry plot and

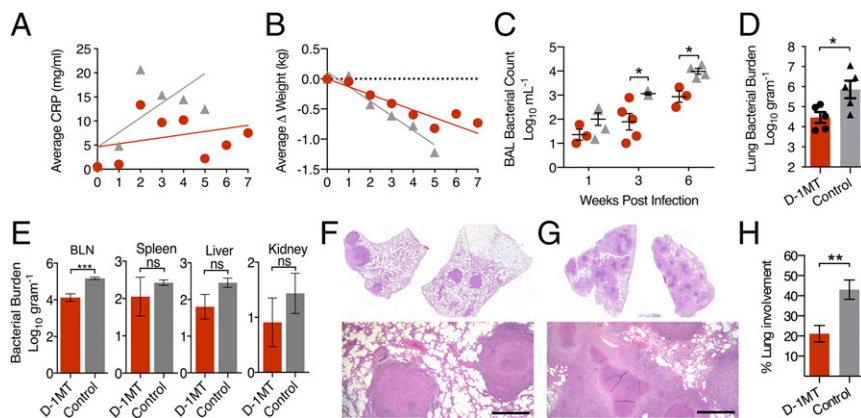


Fig. 2. Clinical, microbiology and pulmonary pathology measures of infection and disease in control and D-1MT-treated macaques. Linear regression of serum CRP (μ g/mL) between two groups (*A*). Linear regression of weight change over the course of time (weeks postinfection) between two groups: D-1MT-treated (orange circle), control (gray circle) (*B*). (*C–E*) Bacterial burdens detected by CFU assay in BAL (*C*), per gram of lung tissues (*D*), and per gram tissue for each BLN, spleen, liver, and kidney (*E*). Subgross H&E staining of lung sections from D-1MT (*F*) and control animals (*G*). (Scale bars, 250 μ m.) Morphometric measure of TB-related total lung pathology (*H*). At least three systematic random microscopic fields from each lung, representing all lung lobes, from at least two of the animals in every group, were used for the morphometric analysis of histopathology. Data are means \pm SEM, * $P < 0.05$, ** $P < 0.01$, *** $P < 0.001$ using (*C*) one-way ANOVA with Bonferroni post correction or (*D*, *E*, and *H*) Student's *t* test; ns, not significant.

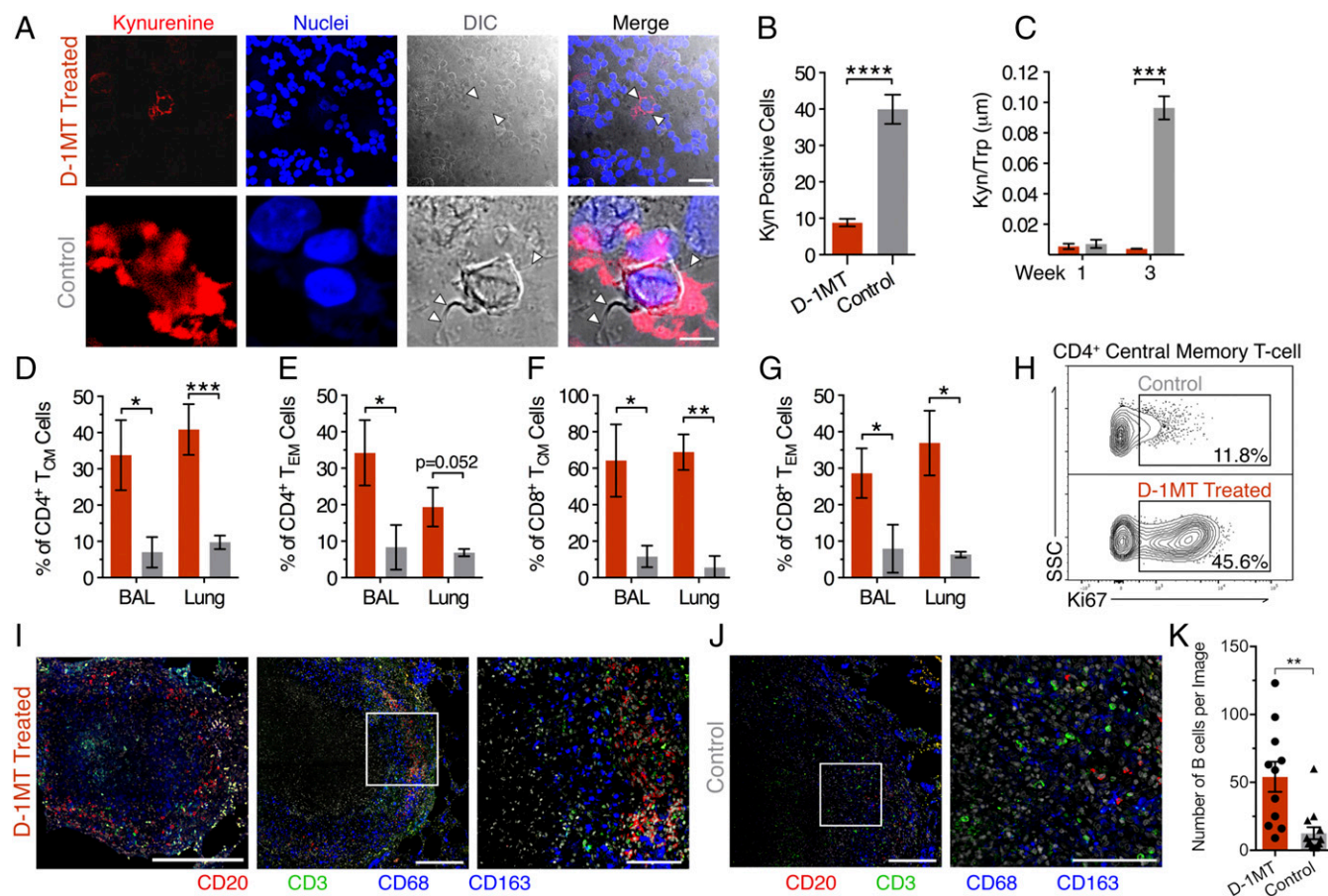


Fig. 3. Assessing the IDO enzymatic activity in *M. tuberculosis*-infected macaques in vivo and its impacts on T and B cell phenotypes. BAL staining 3 wk after *M. tuberculosis*-infection; red, Kyn; blue, nuclei; gray, DIC marked with white arrowheads pointing toward the lining that appears a cell membrane indicates Kyn deposition within a cell. [Scale bars, 100 μ m (Upper); 20 μ m (Lower).] (A) Kyn quantification (B) and Kyn/Trp ratio by ELISA (C). In A, images are shown at different scale with more number of cells in a field from D-1MT-treated animals. Phenotype of memory T cells in BAL and lung samples at necropsy with respect to proliferation as measured by K_i67 positivity in D-1MT-treated (orange) and control animals (gray) (D–H). A representative flow-density plot from lungs of memory T cells expressing K_i67 (H). Costaining with CD20 and CD3 exhibits iBALT in D-1MT-treated (I), control animals (J): red, CD20⁺ B cells; green, CD3⁺ T cells; blue, macrophages. [Scale bars, 20 μ m (I, Left and Right, and J, Right); 40 μ m (I, Middle and J, Left).] White box indicates CD3⁺ T cells (I) and CD20⁺ B cells (J) found in iBALT follicle. Quantification of B cells in the multiple lesions from both groups: D-1MT-treated (orange circle) and control (gray circle) (K) (means \pm SEM). * P < 0.05, ** P < 0.01, *** P < 0.001, **** P < 0.001 using a (B and K) Student's *t* test or (C) two-way ANOVA or (D–G) repeated-measures *t* test.

gating strategy are shown in Fig. S3. Comparisons were also made to T cell phenotypes in peripheral blood (Fig. S4) and immune cell numbers in blood, BAL, and lung (Figs. S4 and S5). We observed significant differences in the percentage of these cells that expressed the highly specific proliferation marker K_i67 (29–32). Thus, the percentage of both central memory (Fig. 3D and F) and effector memory (Fig. 3E and G) cells was higher in BAL as well as lungs of D-1MT-treated animals compared with controls, with enhanced CD4⁺ T_{CM} proliferation, detected by K_i67 , in the treated group (Fig. 3H). Moreover, this difference in T cell proliferation between the two groups could also be observed in peripheral blood ($P = \sim 0.05$) (Fig. S4). Similarly, the K_i67 ⁺ status of central memory CD4⁺, CD8⁺, and effector memory CD8⁺ cells was also significantly enhanced ($P < 0.05$) in the peripheral blood of D-1MT-treated animals relative to control animals (Fig. S4). However, no differences were observed between the two groups of animals in the total number of CD4⁺ or CD8⁺ cells in blood (Fig. S4 E–G), in BAL before or after D-1MT treatment (Fig. S5 A–D) or in the lung (Fig. S5 E–G), except that significantly higher levels ($P < 0.05$) of CD8⁺ T_{EM} cells were present in D-1MT animals at the end point (Fig. S5H). As it is well established that Trp catabolism orchestrated by IDO1 inhibits T cell proliferation (33, 34), mediated directly by end products of this pathway (34), we propose that inhibition of T cell proliferation by IDO1 is one of

the primary mechanisms of Trp catabolism-mediated immune dysfunction in the context of *M. tuberculosis* infection.

D-1MT Induces Inducible Bronchus-Associated Lymphoid Tissue Formation.

We next analyzed the potential effects of D-1MT treatment on inducible bronchus-associated lymphoid tissue (iBALT) formation. The presence of granuloma-associated iBALT is correlated with protection from *M. tuberculosis* infection (13). Paraffin-embedded lung samples collected at the time of necropsy were assayed for iBALT by histopathology and immunofluorescence staining with CD3 (detects T cells) and CD20 (detects B cells) antibodies, followed by confocal microscopy and image analysis (13). The presence of B cells and their follicular organization were greater in D-1MT-treated animals (Fig. 3I) relative to control animals (Fig. 3J). The total number of B cells enumerated in multiple lesion sections of lung was significantly higher ($P = 0.0013$) for D-1MT-treated animals compared with controls (Fig. 3K). These results further support our previous observations that protection from *M. tuberculosis* infection directly correlates with the presence of granuloma-associated iBALT (10, 13, 19, 22).

IDO Inhibition in Vivo Causes Broad-Spectrum Improvement in Granuloma Function. We assessed if IDO inhibition improved the function of granulomas in effectively controlling *M. tuberculosis*

(Fig. 4 and Figs. S6 A–D and S7 A and B). Host genes involved in the proinflammatory cytokine storm and especially the NF- κ B network were induced to higher levels in controls relative to D-1MT-treated animals, highlighting the acute nature of infection in that group (Fig. 4A, two left-most heat maps). The expression of a majority of type I IFN signaling/neutrophil response genes, which are well-characterized biomarkers of active TB (35), was also higher in controls (Fig. 4A). Supervised analyses further revealed signatures of elite granuloma performance in D-1MT-treated animals. These responses were associated with a reduction in T cell inhibitory signaling, including the immune checkpoint inhibitors LAG3, CTLA4, IDO1, CD27, and CD244, and so forth, all of which exhibited lower expression in D-1MT-treated animals (Fig. 4A). LAG3 expression was detected in CD3⁺ as well as CD3⁻ T cells (Fig. S7 A and B). LAG3 is expressed on populations of activated T cells, such as Tregs and NK cells (23, 36), and in the lymphocyte-rich outer layer of the granulomata during ATB (23), and contributes to the reprogramming of the Th1 response (37). Such an environment is likely to be supportive of *M. tuberculosis* persistence rather than its clearance. Concomitantly, the lungs of treated animals presented with a signature of enhanced T cell stimulation and function: for example, increased CCR5 [involved in cross-talk between T cells and macrophages via its ligands CCL16 and CCL8 (38, 39)], CCL25 [involved in T cell development (40)], and NFATC [involved in the maturation of robust anti-*M. tuberculosis* Th1 responses (41)] expression. This was accompanied by increased growth receptor and calcium signaling, signifying a rapidly proliferating thymocyte population (Fig. 4A). In contrast, the lungs of control animals exhibited correlates of T cell dysfunction and exhaustion (Fig. 4A), in agreement with other recent work (42). These results indicate that T cell dysfunction and exhaustion in control animals leads to better *M. tuberculosis* survival than in treated animals ($P < 0.05$) (Fig. 2E).

The lungs of D-1MT-treated animals concomitantly also expressed more intense antimicrobial responses, characterized by induction of certain CD8⁺ T cell genes: for example, CTSB (increased by ~1.3-fold) and other related cathepsins essential for CD8 cytotoxic function (43). In the B cell module, BTK, which is involved in promoting B-cell development and maturation (44), was enhanced 3.3-fold by D-1MT treatment. On the other hand, ETS1, which is involved in down-regulating B cell differentiation (45), was induced by 21-fold in controls compared with D-1MT-treated lungs. Thus, the robust expression of antimicrobial genes, such as cathelicidin antimicrobial peptide, cathepsin B, lysosomal vATPase, and RAB39, in D-1MT-treated animals (Fig. 4A) further underscored our point that suppression of IDO elicits a stronger host response during infection. Most of these genes were either down-regulated or their expression was reduced in control animals.

Several other genes that have positive effects on T cells, either by differentiation or activation, were also induced in D-1MT-treated animals relative to controls (Fig. 4A). On the other hand, genes that negatively affect T cells, either through regulating effector function or survival, were more highly expressed in control animals. The higher expression of genes in the apoptosis module in the treated group was particularly interesting; despite higher T cell proliferation (~46% in D-1MT-treated animals compared with ~12% in control animals) (Fig. 3), the total T cell counts were indistinguishable between the two groups (Fig. S4 E–G). The expression of NR4A1, which encodes a regulator that promotes T cell apoptosis (46, 47), was induced in the lungs of D-1MT-treated animals (Fig. 4A). These microarray results suggest that the highly proliferative thymocytes being recruited to the lungs of D-1MT-treated animals exhibited apoptosis-mediated turnover.

In addition to several pathways related to T cell proliferation, differentiation, and apoptosis, the induction of type I IFNs (Fig. 4A) in BAL confirms the lung data (Fig. 4B) from D-1MT-treated animals. Selected results were validated by qRT-PCR, which confirmed that IDO1 mRNA levels were reduced (by ~50%) in the BAL (Fig. S6B) and lungs (Fig. 4B) of D-1MT-treated animals compared with control animals. Whereas the expression of IDO2 and IFN- γ was not statistically different in both BAL (Fig. S6C) and lungs (Fig. 4B) in treated animals, rel-

ative to untreated animals, the IFN- γ levels approached near significance ($P = 0.0582$) between the two groups in BAL. By RT-PCR, the expression of type I IFN, IFN- β was significantly induced ($P < 0.05$) both in the lungs (Fig. 4B) and BAL (Fig. S6D) of the D-1MT-treated animals. However, we did not detect an induction in the IFN-inducible downstream genes—such as IFIT-1, IFIT-2, IFI44, and so forth—either by microarrays (Fig. 4A) or RT-PCR (Fig. S6 F–H). D-1MT treatment not only alters the host immune responses, but presented with differential B cell and apoptosis signatures (Fig. 4A). Treatment also correlated with altered tissue remodeling, as represented by the up-regulation of several MMPs, IL-8, PAK3, and TIAM (13, 48) (Fig. 4A). IL-8 not only augments the ability of leukocytes to phagocytose and kill bacilli, but it also governs T cell recruitment, thus potentially enhancing immunity to *M. tuberculosis* infection (49). Transcriptomics suggested greater T cell apoptosis in D-1MT-treated animals, and so to verify this we immunostained for the T cell receptor CD3 and performed a TUNEL assay. Immunostaining revealed that animals treated with D-1MT exhibited greater T cell apoptosis (Fig. 4D and E), explaining why there was a comparable number of T cells in both groups (Figs. S4 and S5), despite the higher T cell proliferation in treated animals (Fig. 3 and Fig. S4).

Inhibition of IDO Permits the Reorganization of the TB Granuloma and Allows CD4⁺ T Cells Access to the Lesion Core. The expression of IDO in *M. tuberculosis*-infected macaques primarily occurred in the myeloid (inner half) ring of the granuloma and colocalized with the CD68⁺/CD163⁺ signal. This result reinforced our belief that antigen-presenting cells (APCs) in the lung express IDO in response to acute *M. tuberculosis* replication. We hypothesized that this may lead to the reorganization of the granuloma, such that the CD4⁺ T cells in the lymphoid (outer half) ring are excluded from the pathogen-rich regions, thereby facilitating greater survival and persistence of *M. tuberculosis*.

Next, since the expression of IDO specifically occurs in the inner myeloid ring of the granulomata, we tested the translocation of T cells to the center of the lesion (necrotic center) in lung granuloma of D-1MT-treated and control animals (Fig. 5). Toward this end, we studied if the demarcation between the necrotic center and the lymphocytic layer was more disrupted in the lesions derived from IDO-inhibitor-treated animals relative to untreated animals where it was well defined (Fig. 5 C and D). We found drastic and significant differences ($P < 0.05$) in the number of CD4⁺ T cells present in the inner half of the center of the lesions derived from D-1MT-treated relative to untreated animals (Fig. 5 D and E). Thus, relative to control animals, the total number of CD3⁺ T cells per lesion and their migration from the lymphocytic layer to the necrotic center of granuloma were higher in D-1MT-treated animals (Fig. 5E). These results clearly indicate that IDO signaling affects T cell infiltration into the necrotic centers of granulomas. However, quantification of cells staining positive for IDO indicated that the numbers in the macrophage layer were indistinguishable between the groups (Fig. S7). Additionally, anti-*M. tuberculosis* staining revealed a higher number of bacilli in the lung lesions derived from control- in comparison with D-1MT-treated animals (Fig. 6). Greater bacillary signal was present in the necrotic center in the treated animals compared with the macrophage-rich layer in control animals (Fig. 6). The effector role of CD8⁺ T cells in the control of *M. tuberculosis* infection has recently been described (10). In the present study, we determined that the proliferation of central and effector memory CD8⁺ T cells was significantly enhanced in D-1MT-treated animals than controls (Figs. 3 and 6). Therefore, we sought to better characterize the phenotype of the lymphocytes migrating toward necrotic lesions (Fig. 5E). Approximately 60% of these cells in lesions from D-1MT-treated animals were found to be positive for granzyme B, which was significantly greater than in controls (Fig. 6). A correlation between the frequency of granzyme-expressing T cells and control of human pulmonary TB has been previously described (50). Granzyme B expression on lymphocytes migrating to the lesion core upon IDO inhibition suggests that the latter controls tissue remodeling events. We speculate that IDO

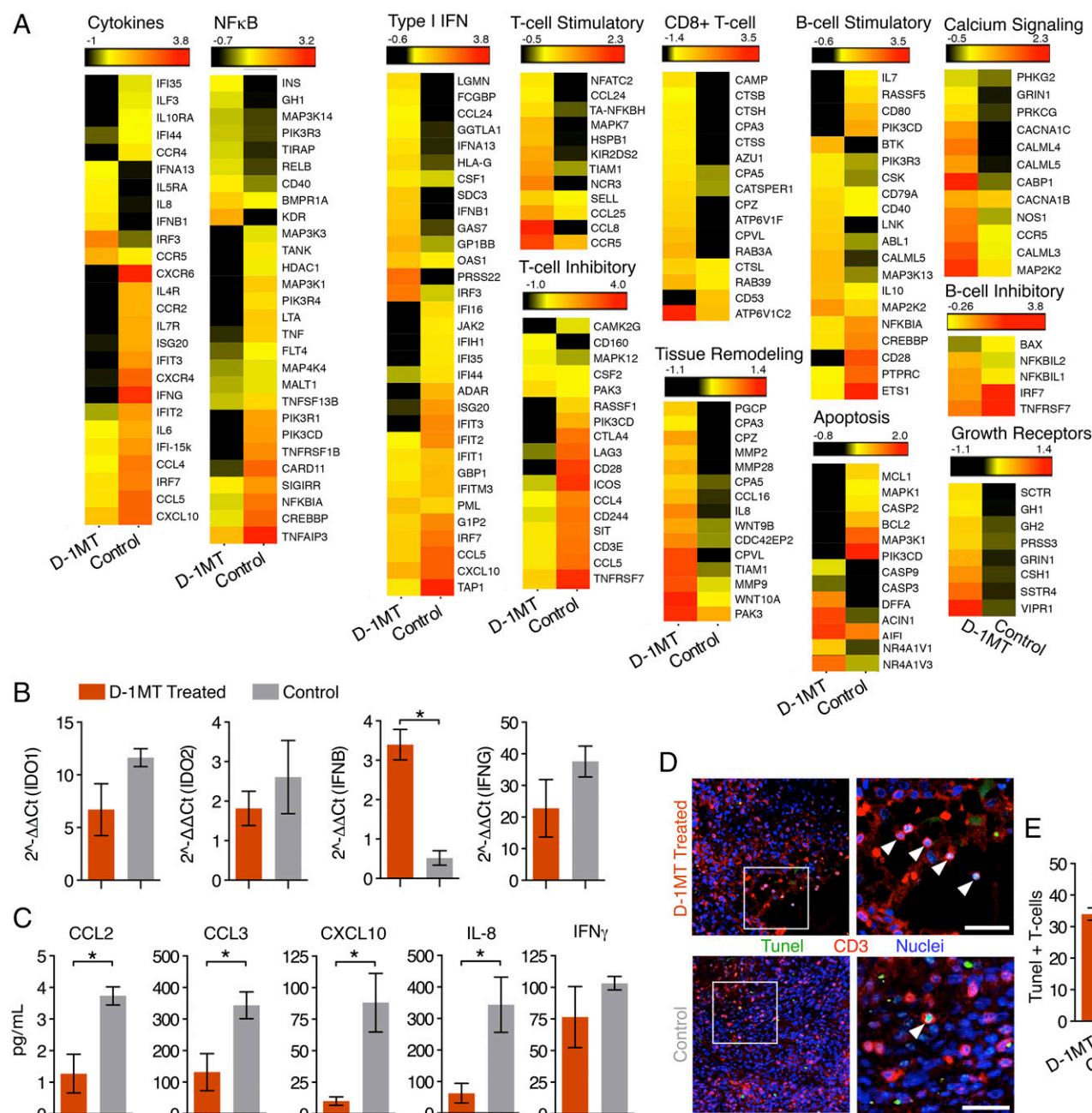


Fig. 4. Impact of inhibiting IDO on lung gene expression. Selected modules derived from significantly enriched pathways based on the method described elsewhere (70) in BAL microarray datasets are shown. The horizontal colored bar on top of each module for a category represents a range in gene-expression magnitude in logarithmic base2. Heat-map clusters: “black” to “yellow” to “red,” lower (fold-change ~ 1.5 cut-off) to higher expression (A). The change in gene expression ($2^{-\Delta\Delta Ct}$) by RT-PCR (B), cytokine assay (C) in lung homogenates of D-1MT-treated (orange) and control animals (gray) relative to uninfected lung samples as base line. GAPDH was used as an internal reference. Bars with no statistics shown are nonsignificant between two groups (e.g., IFN- γ) ($P = 0.3381$) (C). Immunofluorescence-based detection of T cell apoptosis by TUNEL assay. The arrowheads (white) in each magnified image indicate apoptotic cells [scale bars, 20 μ m (Right); magnification, 20 \times (Left)] (D). Data obtained by counting multiple fields with T cells positive for TUNEL staining using a Leica confocal microscope (Leica Microsystems) (E). The data (means \pm SEM) from animals from both groups were used for analysis; * $P < 0.05$, **** $P < 0.001$ using a Student’s t test.

inhibition permits lymphocytes with cytotoxic phenotype to migrate to the center of the tuberculoma and assist in the control of *M. tuberculosis* replication. It is possible that some of these cells may be classic CD8⁺, but the role of other CD3⁺ populations, such as NKT cells and mucosal-associated invariant T cells, cannot be ruled out. These results indicate that intragranulomatous T cell function is radically altered by D-1MT-mediated inhibition of IDO activity.

We conclude that blockade of IDO signaling leads to significantly better control of *M. tuberculosis* infection and reduces the

signs of TB disease by promoting the proliferation of memory T cell subtypes and by enhancing the ability of granulomas to kill *M. tuberculosis*. Because of the possibility that disruption of granuloma following D-1MT treatment might lead to increased dissemination of *M. tuberculosis* to extrapulmonary tissues, we performed CFU assays in BLN, liver, kidney, and spleen at the time of necropsy. The CFU counts in these organs revealed lesser bacterial burdens than controls; however, these numbers were statistically insignificant in liver, kidney, and spleen but drastically reduced in BLN in

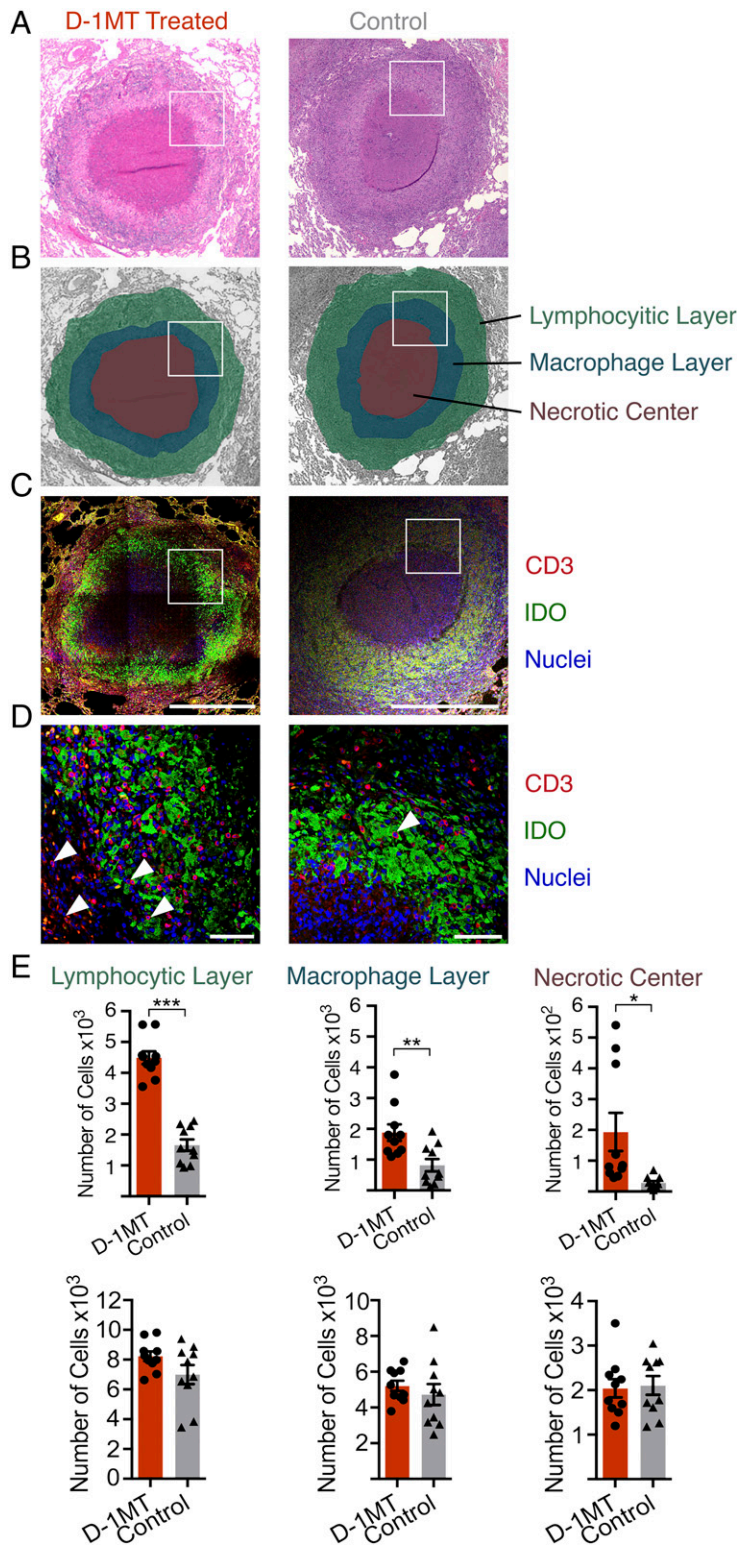


Fig. 5. Extensive relocation of T cells to the internal regions of the macaque granulomata after inhibition of IDO-signaling. H&E staining of a representative lesion from D-1MT-treated (*Left*) and control (*Right*) groups is shown (*A*). A schematic representation of the granulomata shown in *A* is drawn in *B*, distinctly differentiating the lymphocytic and macrophage layers from the necrotic center. The expression of IDO was measured as a function of its presence in either of the three intragranulomatous compartments (necrotic, macrophage, or lymphocytic layer) by immunostaining; IDO (green), CD3 (red), and nuclei (blue) (*C*). A magnification of the white square area in *C* is shown in *D*, with white arrowheads pointing to CD3⁺ cells in red. The number of CD3⁺ cells (*E*, Upper) as well as total nuclei (*E*, Lower) in multiple granulomata in D-1MT-treated (orange with circular data points) and control (gray with triangle data points) animals enumerated in the lymphocytic, macrophage, and necrotic center compartments are shown. For quantification, 10 fields from each compartment were counted under a fixed magnification (corresponding to an area of 0.05 mm²) using a multispectral imaging camera (CRI Nuance). The data are means \pm SEM, **P* < 0.05, ***P* < 0.01, ****P* < 0.001 using a Student's *t* test. [Scale bars, 20 μ m (*C*, also applies to *A* and *B*); 5 μ m (*D*).]

comparison with controls (Fig. 3*F*). Thus, CFU measurements ruled out that disruption of granuloma by D-1MT treatment does not cause an increase in bacterial dissemination to extrapulmonary tissues, but indeed, these animals have over all lesser bacterial burdens.

Inhibition of IDO Signaling in Macrophage: CD4⁺ T Cell Cocultures Restricts Mycobacterial Growth. We cocultured *M. tuberculosis*-infected rhesus macrophages where IDO expression had been

silenced, with *M. tuberculosis*-specific CD4⁺ T cells in vitro, and measured bacterial burden (Fig. S1) used were from rhesus macaques with acute TB infection. The siRNA specifically affected IDO1 (Fig. S1*F* and *J*) and not IDO2 (Fig. S1*F* and *K*) expression. IDO1 silencing resulted in a greater control of *M. tuberculosis* replication when macrophages were cocultured with CD4⁺ T cells but not in macrophages alone (Fig. S1*E*). The silencing of IDO1 resulted in increased levels of IFN- β (Fig. S1*F*

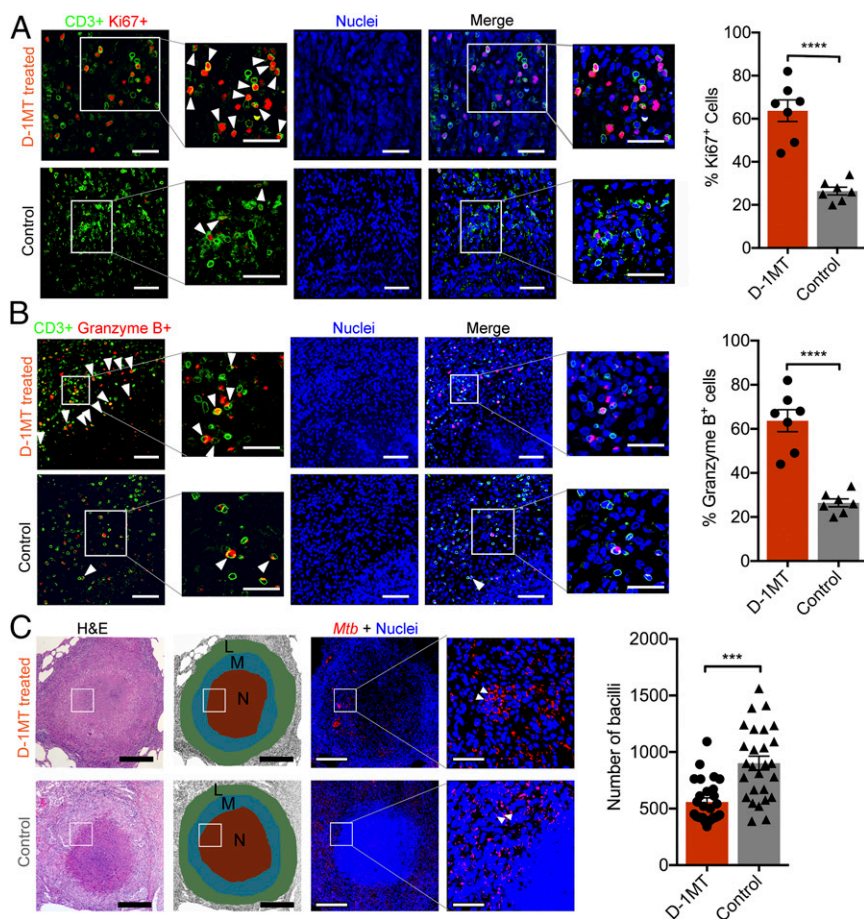


Fig. 6. Granuloma performance in D-1MT-treated and control animals. Immunohistochemistry staining of lung sections for CD3⁺ T cells; (A) Ki67 (red), (B) granzyme B (red) with CD3 in green and nuclei (TOPRO3) stained in blue (A and B) and *M. tuberculosis* (red) staining (C). Multiple granzyme B⁺ cells can be observed in the necrotic center of granuloma from D-1MT-treated animals and are marked with white arrowheads. The far-right images in each panel are close-ups of the boxed region. (Scale bars, 150 μ m.) The total number of cells positive for both CD3 and Ki67 as well as CD3 and granzyme B in A and B, respectively, as well as total nuclei in each panel were counted in multiple granulomata for each group and plotted. The graphs (far right in each panel) show percentages of cells positive for Ki67 (A) and granzyme B (B). The H&E staining of a representative lung lesion from D-1MT-treated (Upper) and control animals (Lower). [Scale bars, 20 μ m (C, H&E); 150 μ m (C, immunostaining).] A schematic representation of the granulomata and demarcation (L, lymphocytic layer; M, macrophage layer; N, necrotic center) in C is shown as described and is also applicable to A and B. The far-right image in C is the close-up of the boxed region and the graph shows the enumeration of bacilli in both groups (C). *** P < 0.001, **** P < 0.0001 using a Student's t test. Data are means \pm SEM, D-1MT treated (orange circle), controls (gray circle).

and L), while the expression of IFN- γ (Fig. S1 F and M) and the internal control GAPDH (Fig. S1 F) was not perturbed.

Discussion

M. tuberculosis utilizes the host granulomatous response to persist in the face of strong immunity (51), by modulating both innate (52) and adaptive (53) immune responses. The fate of *M. tuberculosis* infection is decided in the granuloma; some lesions affect elite control of *M. tuberculosis* replication via enhanced killing, but others fail, resulting in uncontrolled replication and spread. Therefore, the potential to modulate granulomatous responses in favor of bacterial killing by enhancing natural immunity using HDT exists (54, 55). These HDT approaches can channel the chronic immune dysregulation displayed by granulomas that fail, resulting in counterproductive lung pathology, into productive responses characterized by sterilization of granulomas.

M. tuberculosis can overcome the restriction imposed by IDO and the resulting Trp insufficiency, by biosynthesizing this amino acid (8). IDO potently suppresses CD4⁺ T cells via a variety of mechanisms, including limiting their proliferation (56), induction of immunoregulatory APCs, and by promoting the differentiation of Th0 cells into Tregs (57, 58). Thus, high IDO activity has been correlated with pathogen burden and sepsis during infection (59),

especially with intracellular pathogens (60), including *M. tuberculosis* (61). Here, inhibition of IDO activity by a potent yet safe inhibitor in macaques led to a slightly better control of *M. tuberculosis* replication, and somewhat reduced pathology and disease severity, accompanied by increased proliferation of CD4⁺ and CD8⁺ memory and effector populations, and the inhibition of lung marker T cell exhaustion and dysfunction. This was associated with reorganization of the granulomata, with T cells otherwise present in the peripheral region of lesions being able to gain greater access to the core region.

It has recently been shown that mycobacterial infection results in the reprogramming of macrophages in the granuloma to a flattened, epithelial phenotype (62). This results in macrophage interdigitation and tighter granulomas. Inhibition of canonical epithelial pathways in the zebrafish model of *Mycobacterium marinum* infection resulted in the dysregulation of the granuloma, along with immune cell access to the lesion core, and reduced bacillary burdens (62). These results, taken together with our study, suggest that the ability of pathogenic mycobacteria to replicate within host lungs is intricately linked to lesion organization, and disruption of this process represents an attractive future strategy for the control of TB.

Our results have implications both for the fundamental understanding of why granulomas are unable to achieve their full potential during *M. tuberculosis* infection and for providing clues to

likely targets of productive HDT against TB, including IDO. These results suggest that the complex and highly ordered architecture of the primate (and human) lung tuberculoma may in fact be beneficial to the pathogen by preventing contact between T cells and pathogen-containing APCs. It may, however, be possible to alter granuloma architecture by inhibiting IDO signaling, and thereby allowing T cells access to the lesion core while also fostering the development of the follicular organization of B cell-containing iBALT. Such lesions appeared to overcome checkpoint inhibition and T cell dysfunction, greatly promoting bacterial killing.

Inhibition of IDO signaling *in vivo*, as well as *in vitro*, enhanced the expression of the type I IFNs, although the expression of all type I downstream genes (e.g., IFIT1, IFIT2, IFIT3, and so forth) was not induced. These results are not surprising, given that IDO can be induced by both IFN- γ as well as type I IFN. This regulation of IDO by type I vs. type II interferons is context- and cell-type-dependent (63). It appears that type I IFN plays a major role in triggering IDO expression in primate alveolar macrophages in the context of *M. tuberculosis* infection, and therefore, inhibition of IDO enzymatic activity likely causes induction of type I IFN gene expression via feedback (63, 64). Whereas type I IFN is an important antiviral mechanism (65), its induction correlates with increased lung pathology and exacerbated disease upon *M. tuberculosis* infection (66). As such, approaches targeting type I IFN signaling have been successfully attempted in experimental models of TB (66). Our data suggest that the concurrent silencing of IDO signaling and type I IFN signaling could lead to a more profound control of TB in macaque (and human) lungs. Furthermore, testing the potential of such HDT alone, as well as concurrently with anti-TB chemotherapy, could pave the way for future clinical applications. Our results suggest that therapeutic strategies aimed at eliminating or reducing the levels of cells with IDO induction following *M. tuberculosis* infection, such as myeloid-derived suppressor cells in the lung, may also result in reduction of TB. Finally, we have not discussed as part of this report the conundrum that IDO expression on nonhematopoietic cells following *M. tuberculosis* infection may indeed have a protective effect for the host, as has been shown in the murine model (67). Moreover, several novel IDO inhibitors are being generated (e.g., Indoximod), and it may be possible in future studies to test if they are preclinically superior to D-1MT in suppressing IDO activity.

Materials and Methods

In Vivo. Ten rhesus macaques were infected with a high dose of *M. tuberculosis* CDC1551 (~200 CFU) via the aerosol route, as described previously (10–16, 23). Five animals were randomly chosen to be in the treatment group and were D-1MT-treated daily, via the oral route with an IDO enzymatic activity inhibitor, D-1MT (45 mg/kg body weight) 1 wk after *M. tuberculosis* infection. The remaining animals served as controls.

NHPs, Infection, Sampling, Killing, and Clinical Pathology. All 10 animals were negative for tuberculin skin test (TST) before infection, but tested positive 3 wk after *M. tuberculosis* infection. Blood and BAL were collected before and after *M. tuberculosis* infection and during the time-course of D-1MT treatment till necropsy. CFUs were measured in BAL 1 wk after *M. tuberculosis* infection and every 2 wk thereafter until the end point. Lung pathology was determined as described previously (11, 15). CFUs were also measured in lung and lymph node tissues derived at necropsy, as described previously (10–16, 23). Humane end points were predefined in the animal-use protocol and applied as a measure of reduction of discomfort as described earlier to kill animals as necessary (10, 11, 13). The Tulane National Primate Research Center Institutional Animal Care and Use Com-

mittee and the Tulane Institutional Biosafety Committee approved all procedures. All animal procedures were performed in strict accordance with NIH guidelines.

Immunostaining and Confocal Microscopy. H&E histology, immunostaining, and confocal microscopy were performed on formalin-fixed, paraffin-embedded tissues, as previously described (5, 10–13, 15, 19, 22, 23, 68–71). Staining for Kyn was performed on fixed (4% formaldehyde) BAL cytospun frozen slides using a Kyn-specific polyclonal antibody (ImmuSmol). For preparation of frozen BAL slides, 0.1–0.5 million BAL cells were cytospun on a positively charged glass slides (Inform; PerkinElmer) at 700 \times g for 7 min at room temperature, followed by washing two times with PBS (1 \times solution; Thermo Fisher Scientific). Slides were kept for evaporation of residual liquid for 10 min followed by addition of 4% PFA (room temperature) and incubation for overnight and stored in -80°C .

ELISA. Trp and Kyn were quantified in blood plasma samples from all animals before infection (baseline) and every week thereafter until necropsy, using a Trp and Kyn ELISA kit strictly as per the manufacturer's instructions (ImmuSmol).

Flow Cytometry. Flow cytometry was performed on whole blood, BAL, and lung samples from all animals, as previously described (10–13, 16, 20, 21, 23, 26). Briefly, memory subsets were established for T cell populations based on CD28 and CD95 coexpression (72), as previously described (11), and subdivided based on CD3⁺, CD28⁺, CD95⁺ subsets being defined as central memory, and CD3⁺, CD28⁻, CD95⁺ being defined as effector memory. Various antibodies and their amount used for staining are described in Table S2.

Cytokine Assay. Cytokine assays were performed in lung samples derived at time of necropsy from D-1MT-treated and control animals, as well as from naïve (not infected with *M. tuberculosis* and untreated) lungs (as baseline) following the procedures described earlier (11, 23, 68–71).

Quantitative Real-Time RT-PCR and Transcriptomics. Total RNA from BAL obtained at baseline and 3-wk after *M. tuberculosis* infection of two representative animals from each group, was amplified using MessageAmp II aRNA Amplification Kit (Thermo Fisher Scientific) and processed for microarray and qRT-PCR, as described previously (11, 13).

In Vitro Culturing. Monocyte derived macrophages (MDMs) were generated from macaque blood and cocultured with CD4⁺s, as described previously (73). A subset of MDMs was treated with IDO1-specific siRNA 24 h before *M. tuberculosis* infection (multiplicity of infection = 10:1) (Table S1) to inhibit IDO1 expression, as described previously (71). Samples were collected at 0 and 24 h post-infection (71) and used for CFU assay, qRT-PCR, and immunocytochemistry.

Statistics. Unless otherwise stated, statistical analyses were performed with Prism v7 (GraphPad). For statistics, either Mantel–Cox (log-rank) survival analysis, Student's *t* test, or a *t* test with repeated-measures or two-way or one-way ANOVA with Bonferroni multiple comparisons was performed. When required, a goodness-of-fit in linear regression was performed for the statistical analysis between two groups.

More details can be found in *SI Materials and Methods*.

ACKNOWLEDGMENTS. We received help from the Tulane University Office of the Vice President for Research's Editing Department in the grammatical as well as scientific editing of this manuscript. We thank the Tulane National Primate Research Center flow cytometry, microarray, real-time PCR, histopathology, confocal microscopy, and cytokine core facilities. This work was supported by Louisiana State University CoBRE Award P30GM110760 (to S.M.); Tulane National Primate Research Centre Pilot Grant P51OD011104 (to S.M.); NIH Grants AI128130, AI127222, and AI127160 (to S.M.), HL106790, AI089323, and AI134240 (to D. Kaushal), AI111943 and AI123047 (to D. Kaushal and J.R.), AI111914 and AI123780 (to D. Kaushal and S.A.K.), and AI058609 (to A.A.L.), from the Wetmore Foundation of Louisiana; and the Tulane National Primate Research Center Office of the Director and a Bridge Fund from the Tulane Office of Vice-President for Research.

- World Health Organization (2016) Global Tuberculosis Report 2016. Available at www.who.int/tb/publications/global_report/gtbr2016_executive_summary.pdf?ua=1. Accessed October 16, 2016.
- Gandhi NR, et al. (2006) Extensively drug-resistant tuberculosis as a cause of death in patients co-infected with tuberculosis and HIV in a rural area of South Africa. *Lancet* 368:1575–1580.
- Foreman TW, Mehra S, Lackner AA, Kaushal D (2017) Translational research in the nonhuman primate model of tuberculosis. *ILAR J*, 10.1093/ilar/ilx015.
- Russell DG, Barry CE, 3rd, Flynn JL (2010) Tuberculosis: What we don't know can, and does, hurt us. *Science* 328:852–856.
- Mehra S, et al. (2013) Granuloma correlates of protection against tuberculosis and mechanisms of immune modulation by *Mycobacterium tuberculosis*. *J Infect Dis* 207:1115–1127.

- Mbongue JC, et al. (2015) The role of indoleamine 2, 3-dioxygenase in immune suppression and autoimmunity. *Vaccines (Base)* 3:703–729.
- Thomas SM, et al. (1993) IFN-gamma-mediated antimicrobial response. Indoleamine 2,3-dioxygenase-deficient mutant host cells no longer inhibit intracellular *Chlamydia* spp. or *Toxoplasma* growth. *J Immunol* 150:5529–5534.
- Zhang YJ, et al. (2013) Tryptophan biosynthesis protects mycobacteria from CD4 T-cell-mediated killing. *Cell* 155:1296–1308.
- Hou DY, et al. (2007) Inhibition of indoleamine 2,3-dioxygenase in dendritic cells by stereoisomers of 1-methyl-tryptophan correlates with antitumor responses. *Cancer Res* 67:792–801.
- Foreman TW, et al. (2016) CD4⁺ T-cell-independent mechanisms suppress reactivation of latent tuberculosis in a macaque model of HIV coinfection. *Proc Natl Acad Sci USA* 113:E5636–E5644.

11. Mehra S, et al. (2015) The DosR regulon modulates adaptive immunity and is essential for *M. tuberculosis* persistence. *Am J Respir Crit Care Med* 191:1185–1196.
12. Mehra S, et al. (2012) The *Mycobacterium tuberculosis* stress response factor SigH is required for bacterial burden as well as immunopathology in primate lungs. *J Infect Dis* 205:1203–1213.
13. Kaushal D, et al. (2015) Mucosal vaccination with attenuated *Mycobacterium tuberculosis* induces strong central memory responses and protects against tuberculosis. *Nat Commun* 6:8533.
14. Dutta NK, et al. (2010) Genetic requirements for the survival of tubercle bacilli in primates. *J Infect Dis* 201:1743–1752.
15. Mehra S, et al. (2011) Reactivation of latent tuberculosis in rhesus macaques by coinfection with simian immunodeficiency virus. *J Med Primatol* 40:233–243.
16. Mehra S, et al. (2010) Transcriptional reprogramming in nonhuman primate (rhesus macaque) tuberculosis granulomas. *PLoS One* 5:e12266.
17. Kaushal D, Mehra S, Didier PJ, Lackner AA (2012) The non-human primate model of tuberculosis. *J Med Primatol* 41:191–201.
18. Kaushal D, Mehra S (2012) Faithful experimental models of human infection. *Mycobact Dis* 2:e108.
19. Gopal R, et al. (2013) S100A8/A9 proteins mediate neutrophilic inflammation and lung pathology during tuberculosis. *Am J Respir Crit Care Med* 188:1137–1146.
20. Dutta NK, McLachlan J, Mehra S, Kaushal D (2014) Humoral and lung immune responses to *Mycobacterium tuberculosis* infection in a primate model of protection. *Trials Vaccinol* 3:47–51.
21. Darrah PA, et al. (2014) Aerosol vaccination with AERAS-402 elicits robust cellular immune responses in the lungs of rhesus macaques but fails to protect against high-dose *Mycobacterium tuberculosis* challenge. *J Immunol* 193:1799–1811.
22. Slight SR, et al. (2013) CXCR5⁺ T helper cells mediate protective immunity against tuberculosis. *J Clin Invest* 123:712–726.
23. Phillips BL, et al. (2015) LAG3 expression in active *Mycobacterium tuberculosis* infections. *Am J Pathol* 185:820–833.
24. Luo Q, Mehra S, Golden NA, Kaushal D, Lacey MR (2014) Identification of biomarkers for tuberculosis susceptibility via integrated analysis of gene expression and longitudinal clinical data. *Front Genet* 5:240.
25. Larsen MH, et al. (2009) Efficacy and safety of live attenuated persistent and rapidly cleared *Mycobacterium tuberculosis* vaccine candidates in non-human primates. *Vaccine* 27:4709–4717.
26. Mothe BR, et al. (2015) The TB-specific CD4(+) T cell immune repertoire in both cynomolgus and rhesus macaques largely overlap with humans. *Tuberculosis (Edinb)* 95:722–735.
27. Belladonna ML, et al. (2007) Immunosuppression via tryptophan catabolism: The role of kynurenine pathway enzymes. *Transplantation* 84(1, Suppl):S17–S20.
28. Mezrich JD, et al. (2010) An interaction between kynurenine and the aryl hydrocarbon receptor can generate regulatory T cells. *J Immunol* 185:3190–3198.
29. Shedlock DJ, et al. (2010) Ki-67 staining for determination of rhesus macaque T cell proliferative responses ex vivo. *Cytometry A* 77:275–284.
30. Blankenship TN, King BF (1994) Developmental expression of Ki-67 antigen and proliferating cell nuclear antigen in macaque placentas. *Dev Dyn* 201:324–333.
31. Soares A, et al. (2010) Novel application of Ki67 to quantify antigen-specific in vitro lymphoproliferation. *J Immunol Methods* 362:43–50.
32. Kaur A, Hale CL, Ramanujan S, Jain RK, Johnson RP (2000) Differential dynamics of CD4(+) and CD8(+) T-lymphocyte proliferation and activation in acute simian immunodeficiency virus infection. *J Viral* 74:8413–8424.
33. Munn DH, et al. (1999) Inhibition of T cell proliferation by macrophage tryptophan catabolism. *J Exp Med* 189:1363–1372.
34. Terness P, et al. (2002) Inhibition of allogeneic T cell proliferation by indoleamine 2,3-dioxygenase-expressing dendritic cells: Mediation of suppression by tryptophan metabolites. *J Exp Med* 196:447–457.
35. Berry MP, et al. (2010) An interferon-inducible neutrophil-driven blood transcriptional signature in human tuberculosis. *Nature* 466:973–977.
36. Poirier N, et al. (2011) Antibody-mediated depletion of lymphocyte-activation gene-3 (LAG-3(+)-activated T lymphocytes prevents delayed-type hypersensitivity in non-human primates. *Clin Exp Immunol* 164:265–274.
37. Durham NM, et al. (2014) Lymphocyte Activation Gene 3 (LAG-3) modulates the ability of CD4 T-cells to be suppressed in vivo. *PLoS One* 9:e109080.
38. Howard OM, Dong HF, Shirakawa AK, Oppenheim JJ (2000) LEC induces chemotaxis and adhesion by interacting with CCR1 and CCR8. *Blood* 96:840–845.
39. Giovarelli M, et al. (2000) Tumor rejection and immune memory elicited by locally released LEC chemokine are associated with an impressive recruitment of APCs, lymphocytes, and granulocytes. *J Immunol* 164:3200–3206.
40. Svensson M, Agace WW (2006) Role of CCL25/CCR9 in immune homeostasis and disease. *Expert Rev Clin Immunol* 2:759–773.
41. Erb KJ, et al. (2003) Mice deficient in nuclear factor of activated T-cell transcription factor c2 mount increased Th2 responses after infection with *Nippostrongylus brasiliensis* and decreased Th1 responses after mycobacterial infection. *Infect Immun* 71:6641–6647.
42. Drewes JL, et al. (2016) Distinct patterns of tryptophan maintenance in tissues during kynurenine pathway activation in simian immunodeficiency virus-infected macaques. *Front Immunol* 7:605.
43. Balaji KN, Schaschke N, Machleidt W, Catalfamo M, Henkart PA (2002) Surface cathepsin B protects cytotoxic lymphocytes from self-destruction after degranulation. *J Exp Med* 196:493–503.
44. Maas A, Hendriks RW (2001) Role of Bruton's tyrosine kinase in B cell development. *Dev Immunol* 8:171–181.
45. Russell L, Garrett-Sinha LA (2010) Transcription factor Ets-1 in cytokine and chemokine gene regulation. *Cytokine* 51:217–226.
46. Cunningham NR, et al. (2006) Immature CD4+CD8+ thymocytes and mature T cells regulate Nur77 distinctly in response to TCR stimulation. *J Immunol* 177:6660–6666.
47. Woronicz JD, et al. (1995) Regulation of the Nur77 orphan steroid receptor in activation-induced apoptosis. *Mol Cell Biol* 15:6364–6376.
48. Hall A (1998) Rho GTPases and the actin cytoskeleton. *Science* 279:509–514.
49. Krupa A, et al. (2015) Binding of CXCL8/IL-8 to *Mycobacterium tuberculosis* modulates the innate immune response. *Mediators Inflamm* 2015:124762.
50. Busch M, et al.; TBnotTB Network (2016) Lipoarabinomannan-responsive polycytotoxic T cells are associated with protection in human tuberculosis. *Am J Respir Crit Care Med* 194:345–355.
51. Russell DG (2013) The evolutionary pressures that have molded *Mycobacterium tuberculosis* into an infectious adjuvant. *Curr Opin Microbiol* 16:78–84.
52. Agarwal N, Lamichhane G, Gupta R, Nolan S, Bishai WR (2009) Cyclic AMP intoxication of macrophages by a *Mycobacterium tuberculosis* adenylate cyclase. *Nature* 460:98–102.
53. Harding CV, Boom WH (2010) Regulation of antigen presentation by *Mycobacterium tuberculosis*: A role for toll-like receptors. *Nat Rev Microbiol* 8:296–307.
54. Napier RJ, Shinnick TM, Kalman D (2012) Back to the future: Host-targeted chemotherapeutics for drug-resistant TB. *Future Microbiol* 7:431–435.
55. Wallis RS, Hafner R (2015) Advancing host-directed therapy for tuberculosis. *Nat Rev Immunol* 15:255–263.
56. Boasso A, et al. (2007) HIV inhibits CD4+ T-cell proliferation by inducing indoleamine 2,3-dioxygenase in plasmacytoid dendritic cells. *Blood* 109:3351–3359.
57. Popov A, et al. (2006) Indoleamine 2,3-dioxygenase-expressing dendritic cells form suppurative granulomas following *Listeria monocytogenes* infection. *J Clin Invest* 116:3160–3170.
58. Sharma MD, et al. (2007) Plasmacytoid dendritic cells from mouse tumor-draining lymph nodes directly activate mature Tregs via indoleamine 2,3-dioxygenase. *J Clin Invest* 117:2570–2582.
59. van der Sluijs KF, et al. (2006) Influenza-induced expression of indoleamine 2,3-dioxygenase enhances interleukin-10 production and bacterial outgrowth during secondary pneumococcal pneumonia. *J Infect Dis* 193:214–222.
60. Makala LH, et al. (2011) Leishmania major attenuates host immunity by stimulating local indoleamine 2,3-dioxygenase expression. *J Infect Dis* 203:715–725.
61. Suzuki Y, et al. (2013) Indoleamine 2,3-dioxygenase in the pathogenesis of tuberculous pleurisy. *Int J Tuberc Lung Dis* 17:1501–1506.
62. Cronan MR, et al. (2016) Macrophage epithelial reprogramming underlies mycobacterial granuloma formation and promotes infection. *Immunity* 45:861–876.
63. Puccetti P (2007) On watching the watchers: IDO and type I/II IFN. *Eur J Immunol* 37:876–879.
64. Hoshi M, et al. (2010) The absence of IDO upregulates type I IFN production, resulting in suppression of viral replication in the retrovirus-infected mouse. *J Immunol* 185:3305–3312.
65. Azzoni L, et al. (2013) Pegylated interferon alfa-2a monotherapy results in suppression of HIV type 1 replication and decreased cell-associated HIV DNA integration. *J Infect Dis* 207:213–222.
66. Mayer-Barber KD, et al. (2014) Host-directed therapy of tuberculosis based on interleukin-1 and type I interferon crosstalk. *Nature* 511:99–103.
67. Desvignes L, Ernst JD (2009) Interferon-gamma-responsive nonhematopoietic cells regulate the immune response to *Mycobacterium tuberculosis*. *Immunity* 31:974–985.
68. Dutta NK, et al. (2012) The stress-response factor SigH modulates the interaction between *Mycobacterium tuberculosis* and host phagocytes. *PLoS One* 7:e28958.
69. Martinez AN, Mehra S, Kaushal D (2013) Role of interleukin 6 in innate immunity to *Mycobacterium tuberculosis* infection. *J Infect Dis* 207:1253–1261.
70. Gautam US, et al. (2014) DosS is required for the complete virulence of *Mycobacterium tuberculosis* in mice with classical granulomatous lesions. *Am J Respir Cell Mol Biol* 52:708–716.
71. Gautam US, et al. (2014) Role of TNF in the altered interaction of dormant *Mycobacterium tuberculosis* with host macrophages. *PLoS One* 9:e95220.
72. Pitcher CJ, et al. (2002) Development and homeostasis of T cell memory in rhesus macaque. *J Immunol* 168:29–43.
73. Phillips BL, et al. (2017) LAG-3 potentiates the survival of *Mycobacterium tuberculosis* in host phagocytes by modulating mitochondrial signaling in an in-vitro granuloma model. *PLoS One* 12:e0180413.

Supporting Information

Gautam et al. 10.1073/pnas.1711373114

SI Materials and Methods

In Vivo. Ten rhesus macaques were infected with a high dose of *Mycobacterium tuberculosis* CDC1551 (~200 CFU) via the aerosol route, as described previously (1–8). Five animals were randomly chosen to be in the treatment group and were D-1MT-treated daily, via the oral route with an IDO enzymatic activity inhibitor, D-1MT (45 mg/kg body weight) after week 1 of *M. tuberculosis* infection. D-1MT has been previously used to assess the impact of IDO on SIV disease progression in macaques (9). The remaining five animals served as controls.

NHPs, Infection, Sampling, Killing, and Clinical Pathology. All animal procedures were approved by the Institutional Animal Care and Use Committee of the Tulane National Primate Research Center (TNPRC) and were performed in strict accordance with NIH guidelines. The TNPRC is accredited by the Association for the Assessment and Accreditation of Laboratory Animal Care and is routinely monitored by the US Department of Agriculture. Infection was performed as described previously using an aerosol exposure modality specifically configured for macaques (1–8). All 10 animals were negative for tuberculin skin test before infection, but tested positive 3 wk after *M. tuberculosis* infection. Blood and BAL samples were collected before and after *M. tuberculosis* infection and during the time-course of D-1MT treatment till necropsy. Serum CRP, a marker for systemic inflammation, correlated with extent of disease in both groups based on the parameters described previously (1–3). CFUs were measured in BAL 1 wk after *M. tuberculosis*-infection and every 2 wk thereafter until and including the end point. Lungs were stereologically sectioned and pathology was determined as described previously (3, 6). CFUs were also measured in lung and lymph node tissues derived at necropsy, as described previously (1–8). For various assays, lung samples obtained from naïve, TST-negative rhesus macaques from the TNPRC colony were used as baseline. Humane end points were predefined in the animal-use protocol and applied as a measure of reduction of discomfort, as described earlier to kill animals as necessary (1–3). Macaques were killed based on Institutional Animal Care and Use Committee-approved guidelines. To minimize any experimental variation, tissues, blood, and BAL samples collected at each time point and during necropsy were immediately processed without storage for downstream applications, such as flow cytometry, CFU determination, and so forth.

Immunostaining and Confocal Microscopy. H&E histology, immunostaining, and confocal microscopy were performed on formalin-fixed, paraffin-embedded tissues as previously described (1–3, 6–8, 10–16). Staining for Kyn was performed on fixed (4% formaldehyde) BAL cytospun frozen slides using a Kyn-specific polyclonal antibody (ImmuSmol). For preparation of frozen BAL slides, 0.1–0.5 million BAL cells were cytospun on a positively charged glass slides (Inform; PerkinElmer) at 700 × g for 7 min at room temperature followed by washing two times with PBS (1× solution; Thermo Fisher Scientific). Slides were kept for evaporation of residual liquid for 10 min followed by addition of 4% PFA (room temperature) and incubation for overnight. On the following day, slides were wrapped in a foil and stored in –80 °C until used. All of the operations were performed at room temperature inside the BSL3 laminar flow. For quantification of LAG-3, K_i67, Granzyme B, and *M. tuberculosis* in the individual lesions, 10–15 fields from multiple

granulomas were counted under a fixed magnification using a multispectral imaging camera (CRi Nuance) and plotted.

ELISA. Trp and Kyn were quantified in blood plasma samples from all animals before infection (baseline) and every week thereafter until necropsy using Trp and Kyn ELISA kit strictly as per the manufacturer's instructions (ImmuSmol). The Trp and Kyn values were extrapolated from respective known standards provided in each kit and the numeric ratio (Kyn/Trp) was calculated and plotted using GraphPad.

Flow Cytometry. Flow cytometry was performed on whole blood, BAL, and lung samples from all animals as previously described (1–3, 5, 7, 8, 16–19). Briefly, memory subsets were established for T cell populations based on CD28 and CD95 coexpression (20) as previously described (3), and subdivided based on CD3⁺, CD28⁺, CD95⁺ subsets being defined as central memory, and CD3⁺, CD28[–], CD95⁺ being defined as effector memory. Various antibodies and their amount used for staining are described in Table S2.

Cytokine Assay. Cytokine assays were performed in lung samples derived at time of necropsy from D-1MT-treated and control animals, as well as from naïve (not infected with *M. tuberculosis* and untreated) lungs (as baseline) following the procedures described previously (3, 8, 10, 12, 15, 16) with minor modifications. Briefly, lung homogenates were prepared in the lysis Buffer [500 mM Tris-HCl, 0.1% (wt/vol) SDS, 0.15% sodium deoxycholate, 1× protease inhibitor mixture, 1× phosphatase inhibitor mixture (Roche)]. For preparation of lung homogenates, 1 mL lysis buffer per 0.2-g tissue was used. Lung homogenates were filtered with 0.22-μm filters (Millipore) before use in cytokine assay using Cytokine Monkey Magnetic 29-Plex Panel kit (Thermo Fisher Scientific), essentially as described previously (10).

Quantitative Real-Time RT-PCR and Transcriptomics. For host-transcriptomics, total RNA isolated from BAL obtained at the preinfection (~1-wk before infection, baseline) and 3-wk after *M. tuberculosis*-infection of two representative animals from each group was subjected to RNA amplification using MessageAmp II aRNA Amplification Kit (Thermo Fisher Scientific) and processed for microarray and qRT-PCR, as described previously (2, 3). The microarray datasets relative to baseline (as above) were subjected to statistical analysis using ANOVA, as previously described (16). The impact of gene-expression profiles in animals from both groups was compared using Ingenuity Pathway Analysis (Ingenuity Systems). The gene families with significant overrepresentation were selected for supervised clustering and pathway analyses using DAVID and as described elsewhere (2, 3). The genes of a significantly overrepresented pathway (from above) were used to generate modules. The qRT-PCR was performed on subset of genes on microarray datasets and for the detection of Trp biosynthetic genes of *M. tuberculosis* (for primer sequences, see Table S1) in triplicates on RNA derived from four animals in both ATB and LTBI groups, following the method described previously (2, 21).

In Vitro Culturing. Macaque whole blood was collected in EDTA tubes (S-Monovette Sarstedt) and monocytes isolated by Histopaque-1077 (Sigma) density gradient centrifugation. MDMs from these samples were used in a coculture model with autologous CD4⁺ T cells (22). A negative-selection process that involves MACS (magnetic-activated cell sorting) with the NHP

CD4⁺ T cell Isolation Kit (Miltenyi Biotec) was used to isolate CD4⁺ T cells as described previously (22). A subset of MDMs was treated with IDO1-specific siRNA 24 h before *M. tuberculosis*-infection (multiplicity of infection = 10:1) (Table S1) to inhibit IDO1 expression as described previously (16). Samples were collected at 0 and 24 h postinfection (16) and used for CFU assay, qRT-PCR, and immunocytochemistry.

- Foreman TW, et al. (2016) CD4⁺ T-cell-independent mechanisms suppress reactivation of latent tuberculosis in a macaque model of HIV coinfection. *Proc Natl Acad Sci USA* 113:E5636–E5644.
- Kaushal D, et al. (2015) Mucosal vaccination with attenuated *Mycobacterium tuberculosis* induces strong central memory responses and protects against tuberculosis. *Nat Commun* 6:8533.
- Mehra S, et al. (2015) The DosR regulon modulates adaptive immunity and is essential for *M. tuberculosis* persistence. *Am J Respir Crit Care Med* 191:1185–1196.
- Dutta NK, et al. (2010) Genetic requirements for the survival of tubercle bacilli in primates. *J Infect Dis* 201:1743–1752.
- Mehra S, et al. (2010) Transcriptional reprogramming in nonhuman primate (rhesus macaque) tuberculosis granulomas. *PLoS One* 5:e12266.
- Mehra S, et al. (2011) Reactivation of latent tuberculosis in rhesus macaques by coinfection with simian immunodeficiency virus. *J Med Primatol* 40:233–243.
- Mehra S, et al. (2012) The *Mycobacterium tuberculosis* stress response factor SigH is required for bacterial burden as well as immunopathology in primate lungs. *J Infect Dis* 205:1203–1213.
- Phillips BL, et al. (2015) LAG3 expression in active *Mycobacterium tuberculosis* infections. *Am J Pathol* 185:820–833.
- Boasso A, et al. (2009) Combined effect of antiretroviral therapy and blockade of IDO in SIV-infected rhesus macaques. *J Immunol* 182:4313–4320.
- Dutta NK, et al. (2012) The stress-response factor SigH modulates the interaction between *Mycobacterium tuberculosis* and host phagocytes. *PLoS One* 7:e28958.
- Gopal R, et al. (2013) S100A8/A9 proteins mediate neutrophilic inflammation and lung pathology during tuberculosis. *Am J Respir Crit Care Med* 188:1137–1146.
- Martinez AN, Mehra S, Kaushal D (2013) Role of interleukin 6 in innate immunity to *Mycobacterium tuberculosis* infection. *J Infect Dis* 207:1253–1261.
- Mehra S, et al. (2013) Granuloma correlates of protection against tuberculosis and mechanisms of immune modulation by *Mycobacterium tuberculosis*. *J Infect Dis* 207:1115–1127.
- Slight SR, et al. (2013) CXCR5⁺ T helper cells mediate protective immunity against tuberculosis. *J Clin Invest* 123:712–726.
- Gautam US, et al. (2014) DosS is required for the complete virulence of *Mycobacterium tuberculosis* in mice with classical granulomatous lesions. *Am J Respir Cell Mol Biol* 52:708–716.
- Gautam US, et al. (2014) Role of TNF in the altered interaction of dormant *Mycobacterium tuberculosis* with host macrophages. *PLoS One* 9:e95220.
- Darrah PA, et al. (2014) Aerosol vaccination with AERAS-402 elicits robust cellular immune responses in the lungs of rhesus macaques but fails to protect against high-dose *Mycobacterium tuberculosis* challenge. *J Immunol* 193:1799–1811.
- Dutta NK, McLachlan J, Mehra S, Kaushal D (2014) Humoral and lung immune responses to *Mycobacterium tuberculosis* infection in a primate model of protection. *Trials Vaccinol* 3:47–51.
- Mothe BR, et al. (2015) The TB-specific CD4(+) T cell immune repertoire in both cynomolgus and rhesus macaques largely overlap with humans. *Tuberculosis (Edinb)* 95:722–735.
- Pitcher CJ, et al. (2002) Development and homeostasis of T cell memory in rhesus macaque. *J Immunol* 168:29–43.
- Gautam US, Mehra S, Kaushal D (2015) In-vivo gene signatures of *Mycobacterium tuberculosis* in C3HeB/FeJ mice. *PLoS One* 10:e0135208.
- Phillips BL, et al. (2017) LAG-3 potentiates the survival of *Mycobacterium tuberculosis* in host phagocytes by modulating mitochondrial signaling in an in-vitro granuloma model. *PLoS One* 12:e0180413.

Statistics. Unless otherwise stated, statistical analyses were performed with Prism v7 (GraphPad). For statistics, either Mantel–Cox (log-rank) survival analysis, Student’s *t* test or a *t* test with repeated measures or two-way or one-way ANOVA with Bonferroni multiple comparisons was performed. When required, a goodness-of-fit in linear regression was performed for the statistical analysis between two groups.

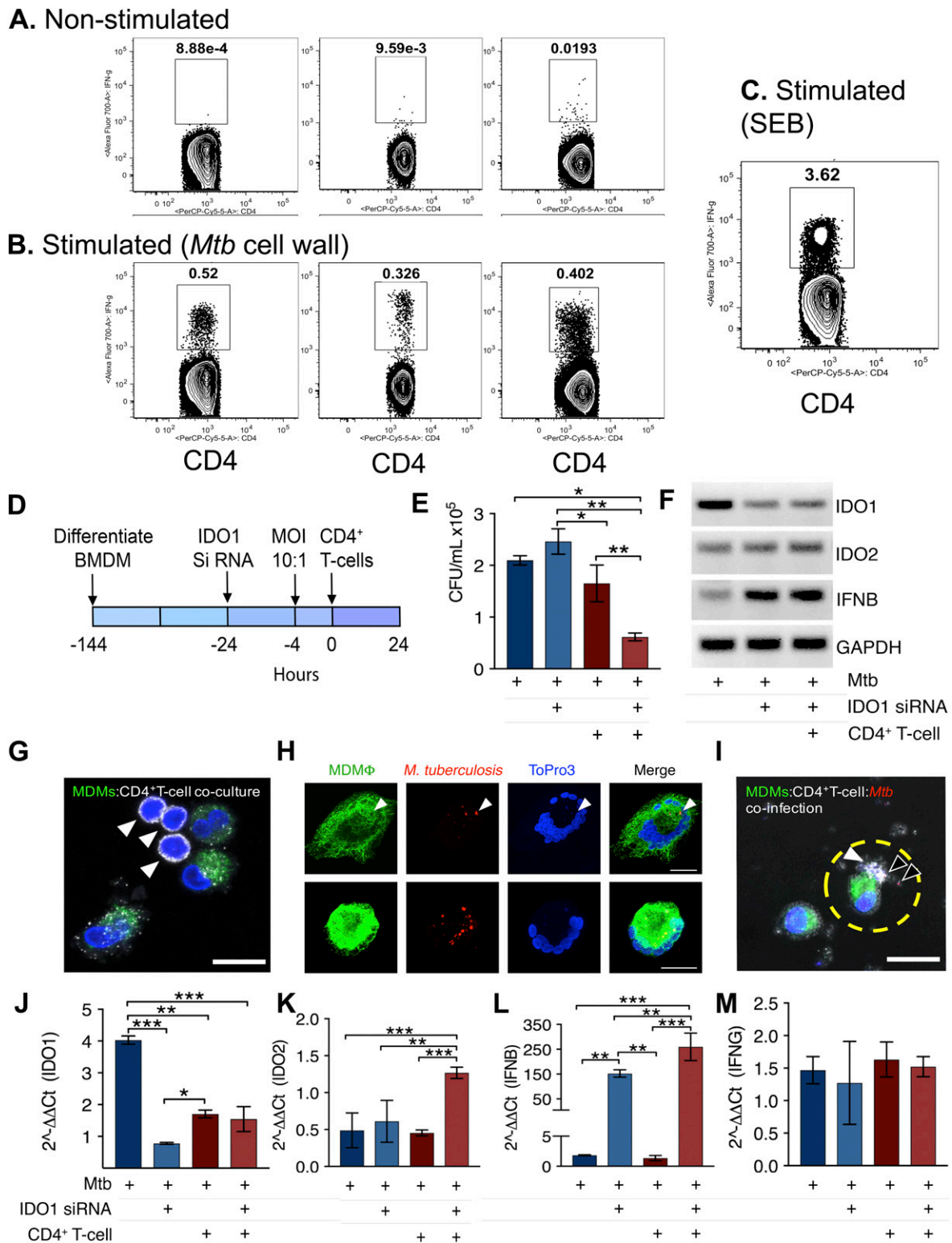


Fig. S1. Analysis of the role of IDO1 during *M. tuberculosis*-infection using MDMs:CD4⁺ T cells in an in vitro coculture model. (A–C) A representative IFN- γ response of CD4⁺ T cells. The CD4⁺ T cells from peripheral blood mononuclear cells prepared from whole blood were used to measure their functional profile, unstimulated (A), and Staphylococcal enterotoxin B (SEB)-stimulated (C) cells are negative and positive controls; *M. tuberculosis* cell wall-stimulated (B). Schematic design (D) of coculture experiment (E–M). MDMs proliferated for 120 h, followed by IDO1 silencing before *M. tuberculosis*-infection (D). CFU measurements at 24 h (E). IDO1 silencing (F and J). Confocal microscopy (G–I) showing immunocytochemical staining of CD4⁺ T cells (white, G and H) MDMs (green), nuclei (blue), and intracellular *M. tuberculosis* (red) marked with white arrowheads. A representative image of an infected macrophage with *M. tuberculosis* (stained in red and shown with black arrowheads in I) associated with T cell indicated with a white arrowhead is shown within a dotted yellow circle in a MDMs:CD4⁺ T cell coculture experiment (I). (Scale bars, 20 μ m.) IDO1 silencing, expression of IFN genes, and bacterial killing in MDMs in the presence of CD4⁺ T cells that were derived from rhesus macaques with acute TB infection (E–M). The qRT-PCR on RNA samples derived at 24 h after *M. tuberculosis* infection to detect IDO1

Legend continued on following page

(F and J), IDO2 (F and K), and interferons; IFN- β (F and L) and IFN- γ (F and M). The gel-electrophoresis-based visual detection of various expression levels of genes; IDO1, IDO2, IFNB, and GAPDH measured by RT-PCR. *M. tuberculosis*-infected MDMs (blue bar), *M. tuberculosis*-infected MDMs with IDO1-specific siRNA (light blue bar), *M. tuberculosis*-infected MDMs cocultured with T cells (dark red bar), and *M. tuberculosis*-infected MDMs with IDO1-specific siRNA and T cells (light red bar). Growth reduction in number of *M. tuberculosis* bacilli (means \pm SEM) in coculture was statistically significant using one way ANOVA, * $P < 0.05$, ** $P < 0.01$, *** $P < 0.001$, **** $P < 0.0001$. Three independent experiments performed in triplicates with samples derived from six rhesus macaques were used for analysis. [Scale bars, 40 μm (G and H); 20 μm (I).]

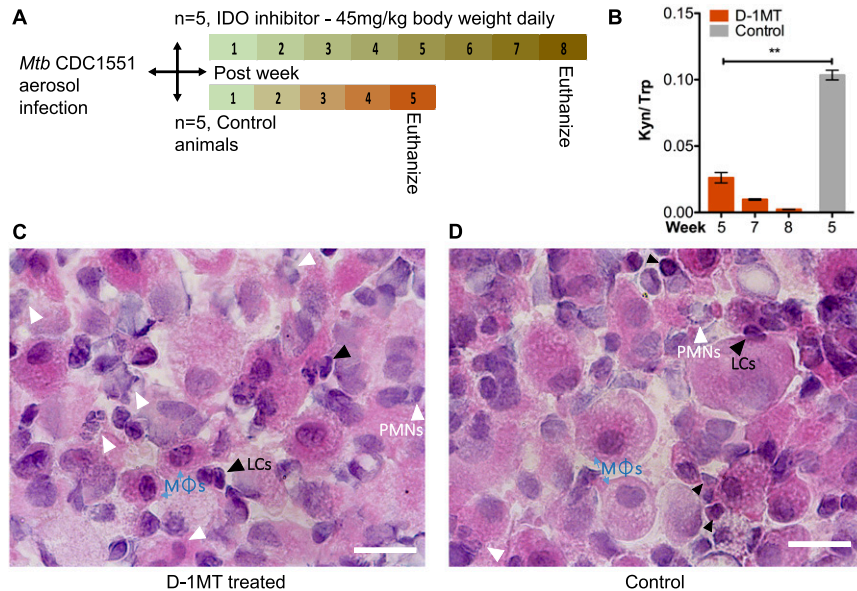


Fig. S2. (A) In vivo study design. A total of 10 Indian rhesus macaques were infected with *M. tuberculosis* CDC1551. Five macaques were treated daily with D-1MT (45 mg/kg body weight) via the oral route, beginning 1 wk after *M. tuberculosis* infection. *M. tuberculosis*-infected but untreated animals served as controls. Blood and BAL were collected every 2 wk after *M. tuberculosis* infection till killing when a complete necropsy was performed for the collection of various tissues and samples for microbiological, biochemical and immunological analyses. (B) Measurement of IDO activity in BAL. Numeric Kyn/Trp ratio in plasma samples between weeks 5–8 after *M. tuberculosis* infection or at necropsy of D-1MT-treated (orange), in comparison with the end point-only time point for the control animals (gray). All five animals in each group were included in the assay and analyses. Data are means \pm SEM, ** $P < 0.01$ using a Student's *t* test. (C and D) H&E staining of BAL cytospin. BAL cytospin samples stained for H&E are shown with vast majority of macrophages present (blue arrows) with few lymphocytes (LC, black arrows) and polymorphonuclear (PMN) leukocytes (white arrows) that are marked in both groups. (Scale bars, 10 μm .)

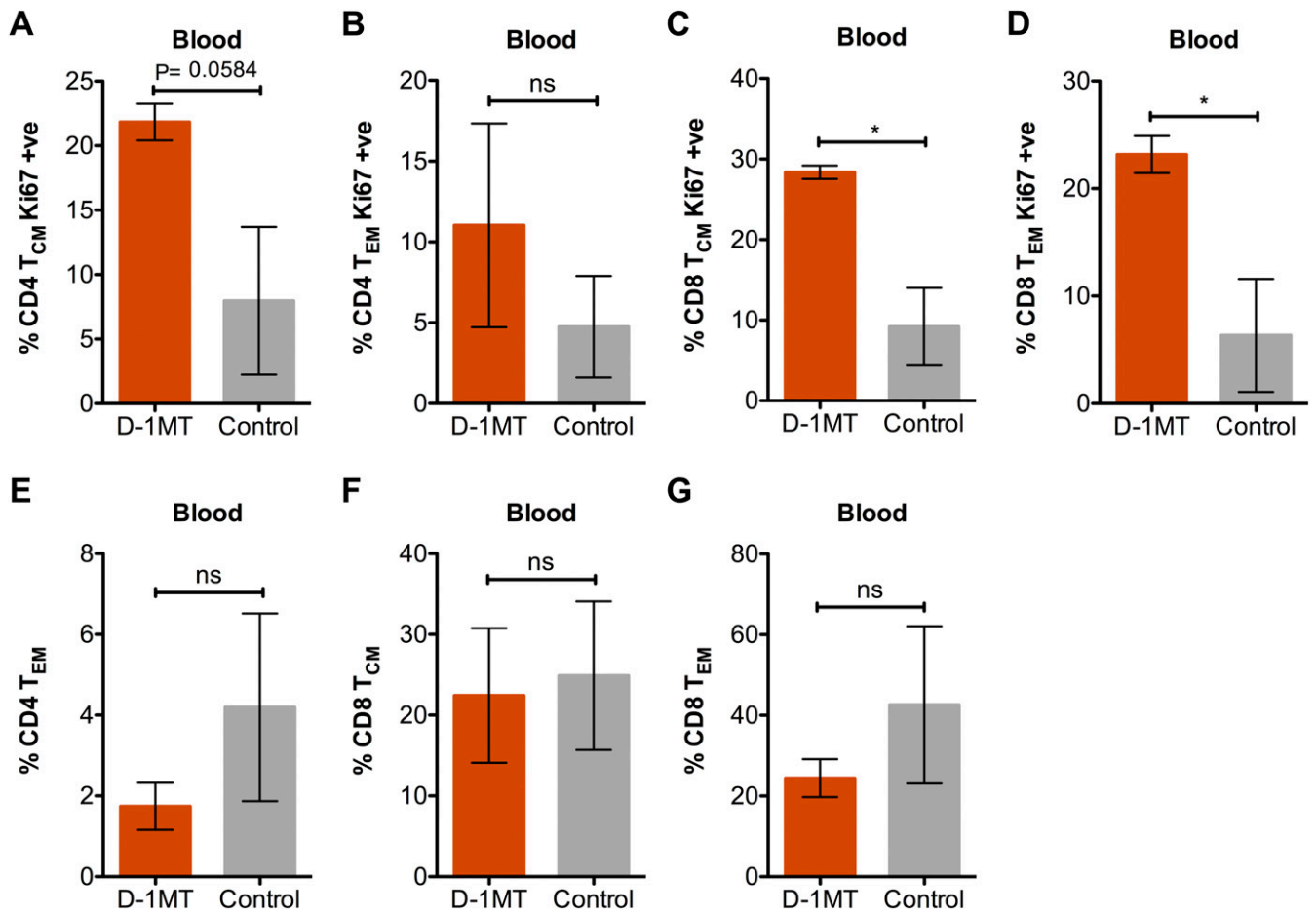


Fig. S4. Flow cytometry based detection of T cell proliferation and T cell counts in blood. (A–D) T cell proliferation. The percentages of CD4⁺ T cell central memory (TCM) and CD8⁺ T cell effector memory (TEM) measured by Ki67 positivity in blood collected at necropsy from both groups; D-1MT (orange) and control (gray). The differences approaching significance ($P = 0.058$) using a Student's *t* test are shown for CD4⁺ TCM in both groups. The data are means \pm SEM, $*P < 0.05$, using a Student's *t* test. The samples at necropsy of five animals each from D-1MT-treated and control groups were included in the analyses. (E–G) T cell counts. Percentages of CD4⁺ effector and both CD8⁺ cell- and effector-memory cells with no significant differences (analyzed using Student's *t* test) obtained in D-1MT-treated and control animals are shown; ns, not significant.

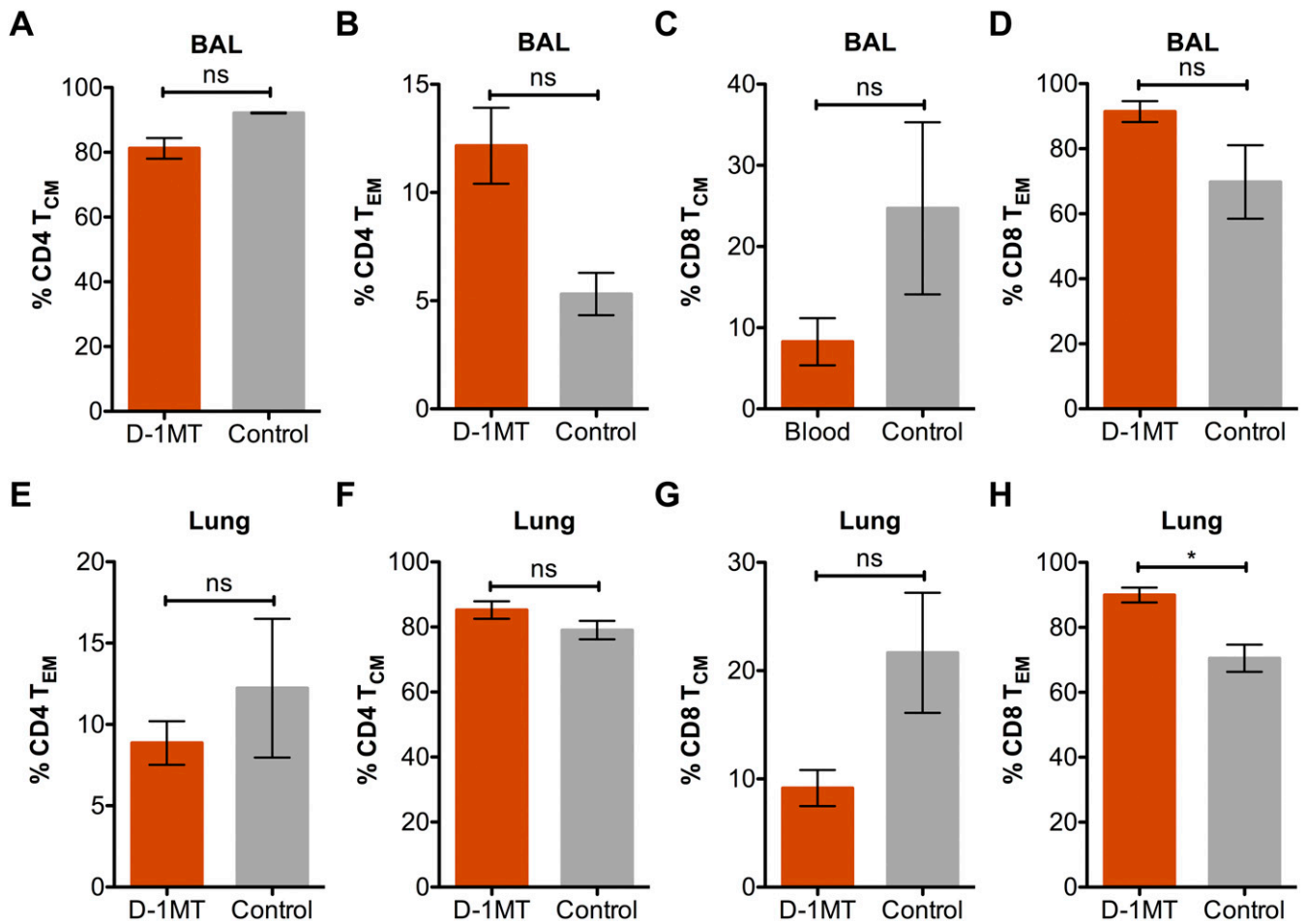


Fig. 55. Flow cytometry-based detection of T cell counts in BAL and lungs. (A–D) T cells counts in BAL. Percentages of T cells in BAL derived at necropsy of D-1MT-treated (orange) and control animals (gray) are shown. The T cell frequencies with no statistical differences for CD4⁺ T_{CM} ($P = 0.0655$), CD8⁺ T_{CM} ($P = 0.1568$), CD4⁺ T_{EM} ($P = 0.0638$), and CD8⁺ T_{EM} ($P = 0.1049$) are shown between two groups of animals. The BAL samples at necropsy of five animals from each group were included in the flow cytometry experiments and analyses. (E–H) T cell counts in lung. Percentages of T cells in BAL derived at necropsy of D-1MT-treated (orange) and control animals (gray) are shown. The differences in T cell frequencies of CD4⁺ T_{EM}, CD4⁺ T_{CM}, and CD8⁺ T_{CM} was insignificant and CD8⁺ T_{EM} was statistically significant ($*P < 0.02$) between two groups using a Student's *t* test. The lung samples at necropsy of five animals from each group were included in the flow cytometry experiments and analyses. ns, not significant.

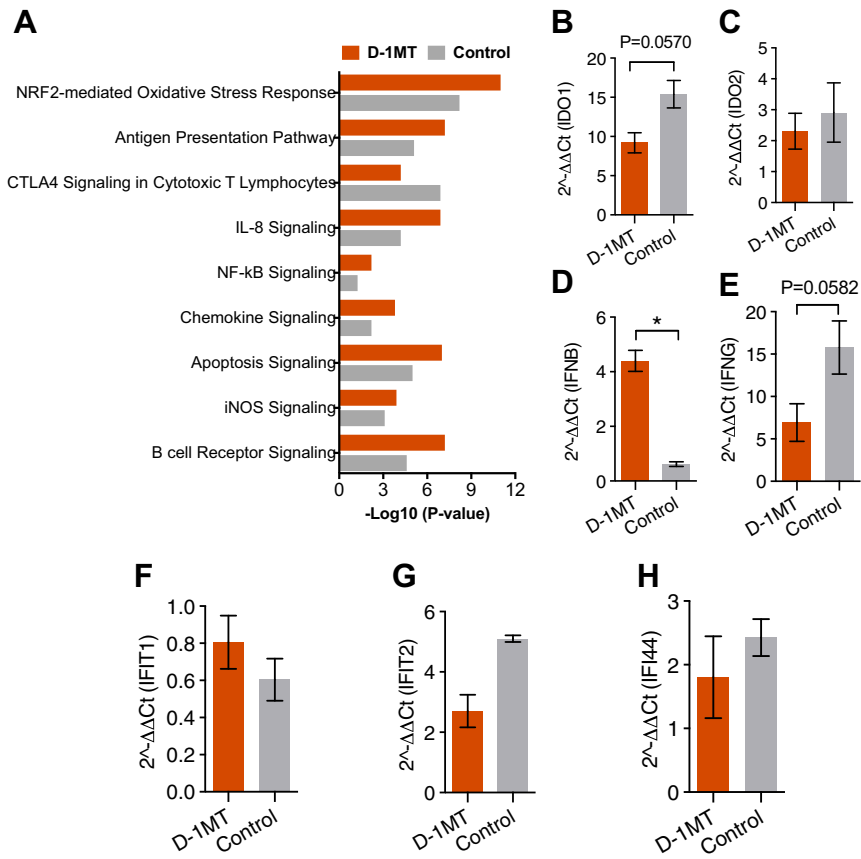


Fig. 56. Transcriptomics in BAL. (A) Microarray-based detection of cytokine signaling pathways in BAL. Gene families with significant overrepresentation as previously described (22), selected for supervised clustering and pathway analyses using DAVID are shown. RT-PCR (B–H). Relative expression (2^{-ΔΔCt}) of IDO1 (B), IDO2 (C), and interferons, IFN-β (D), IFN-γ (E), IFIT1 (F), IFIT2 (G), IFI44 (H) detected at week 3 postinfection; D-1MT-treated (orange) and control animals (gray). The data obtained are significant (**P* < 0.05) for IFN-β or approaching significance for IFN-γ (*P* = 0.0582) or for IDO1 (*P* = 0.0570) and not IDO2, IFIT1, IFIT2, or IFI44 using a student's *t* test. The BAL samples of three animals from each group were included for the analyses.

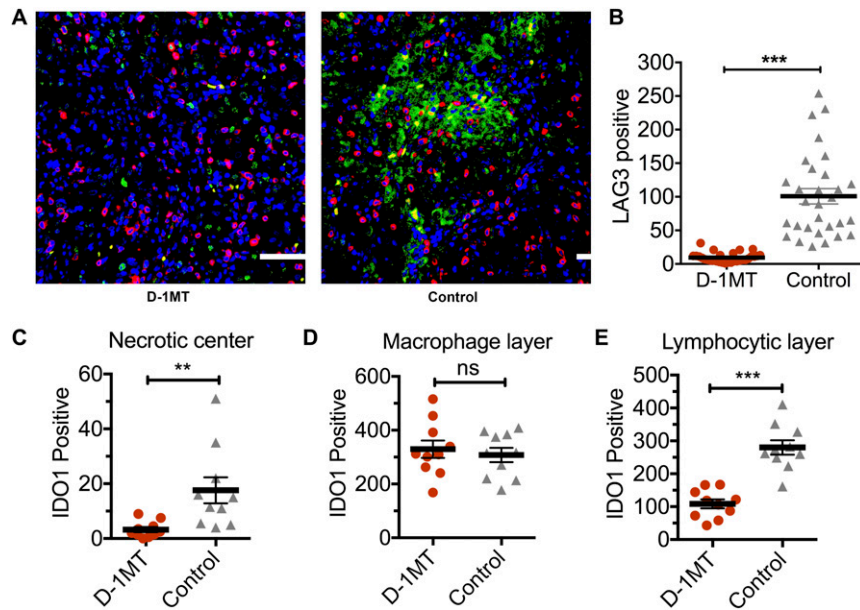


Fig. 57. Detection of LAG3 and IDO1 deposition in lungs by immunohistochemistry. Immunofluorescence based staining of LAG3 (green), CD3⁺ T cells (red), and nuclei (blue) in lungs of D-1MT-treated and control-animals (A). The data obtained by counting multiple fields for cells positive for LAG3 between two groups (orange, D-1MT-treated; gray, control) using Leica confocal microscope (Leica Microsystems) was plotted using GraphPad (B). The data are means \pm SEM, *** $P < 0.0001$ using a Student's t test. Quantification of IDO deposition in the granulomata (C–E). Cells that stained positive for IDO1 in granulomata of animals from two groups; D-1MT-treated (orange) and control (gray) were enumerated in the various compartments: the lymphocytic layer (C), macrophage layer (D), and necrotic layer (E) (also see Fig. 5 for distribution of these layers within granuloma). The data obtained by counting IDO⁺ cells (C–E) in multiple fields and granuloma were significant for the lymphocytic layer ($P < 0.0001$) and necrotic center (** $P < 0.05$) using a student's t test, or these numbers were not different in the macrophage layer in the lesions derived from two groups of animals. ns, not significant. (Scale bars, 20 μm.)

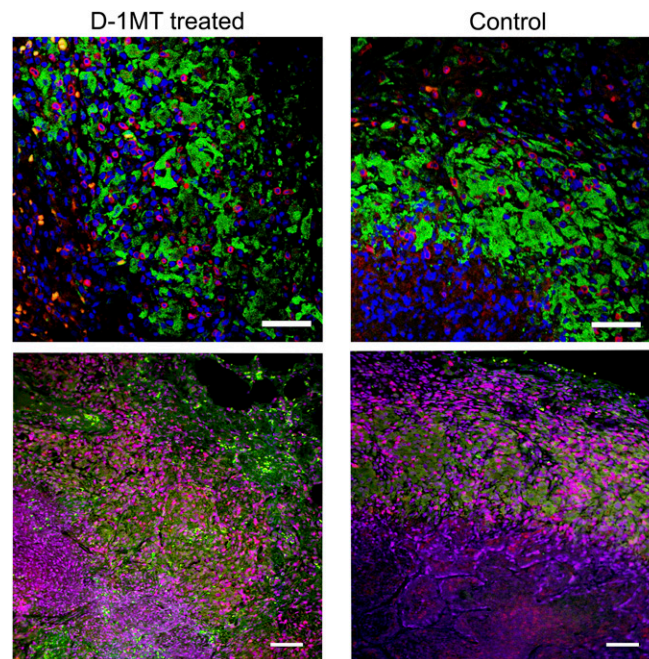


Fig. 58. Immunohistochemistry of lung sections derived from D-1MT-treated and control animals; IDO1 (green), CD3 (red), and nuclei (blue). [Scale bars, 20 μm (Upper); 40 μm (Lower).]

Table S1. Primers and siRNA used in the study

Gene/siRNA	Primer/siRNA sequence (5'-3')
Rh IDO1 F	GGTTTATGCAGACTGTGTCTTGGCA
Rh IDO1 R	CTCCATCACGAAAGGAGAACAAAAAC
Rh IDO2 F	CAGATTCTCTGAAAGAAGCTCCAGAT
Rh IDO2 R	ACATGAGCTCGAAGCTGGTGAGC
Rh IFN- γ F	GACTCGAATGTCCAACGCAAAGCA
Rh IFN- γ R	CGACCTCGAAACATCTGACTCCTTT
Rh IFN- β F	ACGCTGCATTGACCATCTATGAGA
Rh IFN- β R	TTAGCAAGGAAGTTCTCCACAATAGT
Rh GAPDH F	TCAAGAAGGTAGTGAAGCAGGCGT
Rh GAPDH R	AAGAGTGGGTGTCGCTGTTGAAGT
<i>Mtb trpE</i> F	GTACCGAATTCTGCGGGTAA
<i>Mtb trpE</i> R	ACAATCGAAAAGTCCACTGC
<i>Mtb trpD</i> F	GAGGTGGGATCGGGTTCT
<i>Mtb trpD</i> R	CCCAGAAAGATTGAACACGG
<i>Mtb trpC</i> F	AATCGTTGGGTATGACAGCA
<i>Mtb trpC</i> R	GTTAACGCCAATCACCTTGG
<i>Mtb trpA</i> F	GCGGCATTGATTGGTTACTT
<i>Mtb trpA</i> R	GGAACCCCGACTTCGATAAT
<i>Mtb trpB</i> F	TAGGTGTTGAGTTGGGAAGG
<i>Mtb trpB</i> R	AGCAAGCCAAACCATTTCG
Rh IDO1 siRNA sense	GGAUAAAGGUCAUGGAGACUU
Rh IDO1 siRNA antisense	GUCUCCAUGACUUUAUCCUU

This table reports the sequences of oligonucleotides and macaque specific IDO1 Si-RNA used in qRT-PCR and cell culture, respectively. The primers were designed from rhesus macaque-specific and *M. tuberculosis*-specific genes. F, forward primer; R, reverse primer; Rh, rhesus.

Table S2. List of antibodies

Fluorochrome	Antibody name	Source	Clone	Quantity used per sample (μ L)	Catalog no.
FITC	CD69	BD Biosciences	FN50	20	555530
PerCP-Cy5.5	CD4	BD Biosciences	L200	20	552838
APC	CD8	BD Biosciences	RPA-T8	10	555369
AL 700	CD3	BD Biosciences	SP34-2	10	557917
APC-HY7	CD20	BD Biosciences	2H7	5	560853
BV421	CD95	BD Biosciences	DX2	5	562616
BV510	Ki67	BD Biosciences	B56	5	563462
BV711	CD28	BD Biosciences	CD28.2	5	563131
PE	CCR5	BD Biosciences	3A9	20	550632

The table summarizes the list of antibodies used for staining by flow cytometry experiments.